TITLE: Sleep is bi-directionally modified by amyloid beta oligomers

AUTHORS: Güliz Gürel Özcan[1], Sumi Lim[1], Patricia L.A. Leighton[2,3], W. Ted Allison[2,3], Jason Rihel[1*]

AFFILIATIONS:

1 Department of Cell and Developmental Biology, UCL, Gower Street, London, United Kingdom WC1E 6BT

2 Centre for Prions & Protein Folding Disease, University of Alberta, Edmonton AB, T6G 2M8, CANADA

3 Department of Biological Sciences, University of Alberta, Edmonton AB, T6G 2E9, CANADA

***CORRESPONDENCE:** j.rihel@ucl.ac.uk

HIGHLIGHTS:

- **Amyloid beta oligomers can drive either sleep or wakefulness, depending on their size**
- **Wakefulness driven by short amyloid beta oligomers requires binding partners Adrenergic Beta Receptor 2 and Pgrmc1**
- **Long amyloid beta oligomers drive sleep through interaction with Prion Protein**
- **The in vivo sleep effects of amyloid beta can be pharmacologically blocked by targeting several steps of the Amyloid beta-Prion Protein signalling cascade.**

SUMMARY:

Disrupted sleep is a major feature of Alzheimer's Disease (AD), often arising years before symptoms of cognitive decline. Prolonged wakefulness exacerbates the production of amyloid-beta (Aβ) species, a major driver of AD progression, suggesting that sleep loss further accelerates AD through a vicious cycle. However, the mechanisms by which Aβ affects sleep are unknown. We demonstrate in zebrafish that Aβ acutely and reversibly enhances or suppresses sleep as a function of oligomer length. Genetic disruptions revealed that short Aβ oligomers induce acute wakefulness through Adrenergic receptor b2 (Adrb2) and Progesterone membrane receptor component 1 (Pgrmc1), while longer Aβ forms induce sleep through a pharmacologically tractable Prion Protein (PrP) signalling cascade. Our data indicate that Aβ can trigger a bi-directional sleep/wake switch. Alterations to the brain's Aβ oligomeric milieu, such as during the progression of AD, may therefore disrupt sleep via changes in acute signalling events.

INTRODUCTION:

Accumulation of amyloid-beta (Aβ) in plaques, along with tau tangles, is one of the two pathological hallmarks of Alzheimer's Disease (AD). Change in Aβ levels in the brain is one of the earliest known pathological events in AD and is detectable years before the development of Aβ plaques and decades before the clinical onset of AD (Bateman et al., 2007; Jack et al., 2013). Because of its importance in AD progression, Aβ has been mostly characterized as a functionless, pathological, intrinsically neurotoxic peptide (Moir and Tanzi, 2019). However, Aβ is an ancient neuropeptide conserved across vertebrates through at least 400 million years of

evolution (Moir and Tanzi, 2019). Aβ's cleavage from Amyloid Precursor Protein (APP) is tightly regulated by multiple enzymatic reactions (O'Brien and Wong, 2011), and its release from neurons is carefully controlled (Kamenetz et al., 2003). Aβ interacts with numerous surface receptors and can activate intrinsic cellular signalling cascades to alter neuronal and synaptic function (Jarosz-Griffiths et al., 2016). More recently, Aβ has been suggested to act as an antimicrobial peptide (Soscia et al., 2010), and the deposition of Aβ may be induced as an innate immune defence mechanism against microbial pathogens (Kumar et al., 2016). However, the various biological effects of Aβ in health or disease remain obscure.

One of the earliest symptoms of AD is the disruption of sleep, and AD patients have sleep-wake abnormalities, including insomnia at night and increased napping during the day (Allen et al., 1987; Loewenstein et al., 1982; Moran et al., 2005; Prinz et al., 1982). Multiple transgenic AD mouse models that overproduce Aβ also show disrupted sleep phenotypes (Roh et al., 2012; Sterniczuk et al., 2010; Wang et al., 2002), often in the absence of neuronal loss and preceding impairments of learning and memory (Irizarry et al., 1997). In non-pathological conditions, Aβ levels in the cerebrospinal fluid (CSF) are modulated by the sleep-wake cycle (Kang et al., 2009; Xie et al., 2013). Aβ generation and release is controlled by electrical and synaptic activity (Cirrito et al., 2005; Kamenetz et al., 2003), leading to increased extracellular Aβ levels during wakefulness and decreased levels during sleep (Kang et al., 2009; Xie et al., 2013). These observations have led to the proposal that sleep and Aβ dynamics create a vicious feed-forward cycle, wherein increases in wakefulness result in increased extracellular Aβ and aggregation, which then dysregulates sleep, further exacerbating pathogenic Aβ production (Roh et al., 2012). How increased Aβ burden leads to disruptions in sleep remains unknown, although AD-related

cell death of critical sleep/wake regulatory neurons has been suggested as a possible mechanism (Fronczek et al., 2012; Lim et al., 2014; Manaye et al., 2013).

Given the relationship between Aβ and sleep, we hypothesized that Aβ may directly modulate sleep-regulatory pathways independently of neuronal cell death. To test this, we took advantage of the ability to directly deliver small molecules and Aβ peptides to the brain of larval zebrafish, which have conserved APP processing machinery and Aβ peptides (Newman et al., 2014) and share genetic, pharmacological, and neuronal sleep-regulatory mechanisms with mammals (Barlow and Rihel, 2017). We found that Aβ size-dependently and reversibly modulates behavior through two distinct genetic, pharmacologically tractable pathways that regulate sleep in opposing directions.

RESULTS:

Aβ dose-dependently modifies zebrafish sleep and wake behavior

Isolating the specific biological effects of Aβ has been experimentally difficult. One challenge is that Aβ is processed from a series of complex cleavage steps of a longer transmembrane protein, Amyloid Precursor Protein (APP), which also produces other protein products with a variety of functions (O'Brien and Wong, 2011). This restricts the utility of genetic manipulations to tease out Aβ-specific roles from the other APP components. Another challenge is that Aβ forms, *in vitro* and *in vivo*, a variety of oligomeric species (e.g. dimers, longer oligomers, or large fibrils) with diverse structures, binding affinities, and signalling properties (Benilova et al., 2012; Jarosz-Griffiths et al., 2016). Teasing out the biological signalling capabilities of these diverse

oligomeric species requires selective manipulation of Aβ oligomeric states, which is difficult *in vitro* and is currently nearly impossible endogenously *in vivo*.

To overcome some of these barriers, we developed an injection assay in which the amount and type of the Aβ oligomers can be controlled and then tested the acute signaling effects of Aβ on sleep and wake behavior. Our minimally invasive intra-cardiac injection assay in 5 days post fertilization (5dpf) larval zebrafish avoids direct damage to brain tissue (Figure 1A and 1B). This technique rapidly (<1hr, peaking within 2-3hrs) and reversibly delivers Aβ to the larval brain, as assessed by injection of fluorescently tagged Aβ42 and subsequent confocal brain imaging (Figure 1B, Figure 1- figure supplement 1A, B). To generate different Aβ oligomeric species, we modified previously established *in vitro* monomeric Aβ incubation protocols (see Extended Methods) that enrich for Aβ with different oligomeric sizes and opposing effects on rat neuronal excitability (Kusumoto et al., 1998; Orban et al., 2010; Whitcomb et al., 2015). By incubating Aβ42 overnight at increasing temperatures, we generated Aβ oligomeric pools with significantly different lengths, as measured by Transmission Electron Microscopy (TEM) (Figures 1C and Figure 1- figure supplement 1C). Aβ42 incubated overnight at 4ºC consisted of fewer and shorter oligomers ($A\beta^{short}$, mean 45±11 nm, median=39nm) than when incubated at 25ºC ($A\beta^{long}$, mean 75±10 nm, median=61nm) or at 37ºC ($A\beta^{v\text{-}long}$, mean 121±10 nm, median=88nm) (Figure 1C).

We then assessed how each Aβ preparation affected sleep and wake behavior in zebrafish relative to an Aβ42-1 “reverse” peptide control ($A\beta^{rev}$) using automated video-monitoring (Prober et al., 2006; Rihel et al., 2010). In initial experiments, we determined the appropriate Aβ injection dose by injecting 1nL of a 1-1000 nM dose series for both $A\beta^{short}$ and $A\beta^{long}$ and

assessing subsequent waking activity and sleep, which is defined in zebrafish larvae as a period of inactivity lasting longer than one minute, which are associated with an increased arousal threshold and other features of behavioral sleep (Prober et al., 2006). Unexpectedly, these oligomeric species had opposing behavioral effects (Figure 1- figure supplement 1D-G). $A\beta^{short}$ increased waking activity and decreased sleep relative to Aβ reverse peptide, while $A\beta^{long}$ decreased waking and increased sleep (prep waking effect, $p<0.001$; prep sleep effect $p<0.05$, two-way ANOVA). These effects were generally consistent across doses, although some dose-responses elicited stronger differential effects than others (Figure 1- figure supplement 1D, E), with the maximal difference between the $A\beta^{short}$ and $A\beta^{long}$ preparations at 10 nM ($p\leq0.01$ doseXprep interaction, two-way ANOVA). We estimate this dose yields a final concentration that falls within the lower range of physiological concentrations reported for Aβ42 in human CSF of 100 pM-5nM (Bateman et al., 2007). For example, assuming that all injected Aβ goes into the brain, the highest possible concentration would be 1500 pg/ml or 300 pM (45 ng/ml x 1 nl in 30.4 nl brain= 1.5 ng/ml=1500 pg/ml). At the lower end, assuming equal distribution of Aβ over the whole body yields a final concentration estimate of 150 pg/ml or 30 pM (45 ng/ml x1 nl in 300 nl of body= 150 pg/ml). We therefore continued with 10 nM injections for all subsequent experiments, as it combines the maximal differentially observed behavioral effects between $A\beta^{short}$ and $A\beta^{long}$ with physiologically reasonable concentrations.

Aβ affects sleep and wake in opposing directions as a function of oligomer size and independently of neural death

To explore the effect of Aβ oligomeric size on sleep, we then systematically tested the behavior effects of each Aβ species relative to a $A\beta^{rev}$ control for n=3-5 independent experiments each.

As in the dose response experiments, Aβ affected sleep and wake in opposing directions depending on its oligomeric state (Figures 1D-1I'). In the day following injection, $A\beta^{short}$ significantly increased waking activity by +12.8% and reduced total sleep relative to $A\beta^{rev}$ by 15.5% (Figures 1D-E'). The magnitude of the sleep effect is likely partially masked by a flooring effect due to generally reduced sleep during the day; we therefore favor reporting effect sizes and confidence intervals as recommended (Amrhein et al., 2019; Ho et al., 2019). Indeed, if we were to combine all the additional control $A\beta^{short}$ experiments subsequently reported in this manuscript (n=160 $A\beta^{rev}$ n=164 $A\beta^{short}$, see Figures 3G and 3H), the effect size remains robust at -15.9% and the result is statistically significant ($p<0.05$, one-way ANOVA). These effects were reversible, as there were no significant differences in sleep (Figure 1E, black bar) or waking activity (Figure 1D, black bar) between $A\beta^{short}$ and reverse peptide in the night following injection, and the behavior of $A\beta^{short}$-injected larvae returned to baseline levels in the subsequent day (Figure 1-figure supplement 3A).

In contrast, while injection of longer Aβ fibers ($A\beta^{v\_long}$) had no effect on behavior, (Figures 1H-I'), injection of the intermediate $A\beta^{long}$ oligomers significantly increased sleep during the post-injection day by +47.2% and reduced waking activity by 11.3% (Figures 1F-1G'). The increased sleep induced by $A\beta^{long}$ was due to a significant increase in the average number of sleep bouts but not an increase in sleep bout length (Figure 1J), indicating higher sleep initiation is responsible for the change in sleep rather than an increased sleep consolidation. This increased sleep effect by $A\beta^{long}$ was not observed in the night following injection (Figures 1F and 1G, black bar), and behavior returned to baseline by the following morning (Figure 1- figure supplement 3B).

This data is consistent with $A\beta^{short}$ increasing wakefulness and $A\beta^{long}$ decreasing wakefulness

and increasing sleep. Additional control experiments ruled out experimental artefacts, as larvae undergoing no treatment, anaesthesia only, mock injection, or PBS only injections had indistinguishable effects on sleep/wake (Figure 1- figure supplement 1H-J). Next, we recalculated the behavioral analysis only for the evening period before lights off, when vehicle-injected larvae were statistically indistinguishable from larvae that had been acclimated to the tracking rig for 24 hours (Figure 1- figure supplement 1J). Except for an even more severe flooring effect in the $A\beta^{short}$ injection experiments, the results from evening-only analysis were indistinguishable from calculations across the whole day (Figure 1- figure supplement 1K). We therefore used full day analysis for all subsequent experiments.

We next considered if the dual-effects of Aβ on sleep and wake are due to either neuronal damage or generalized toxic effects, such as the induction of seizure, paralysis, or sickness behavior.

First, injection with either long or short forms of Aβ had no effect on apoptosis, as detected by staining for activation of Caspase-3 (Figure 1- figure supplement 2A-C). In addition, Aβ injected animals raised to adulthood showed no major differences in their general health or in their survival rates (Figure 1- figure supplement 2D). Moreover, injected animals recovered fully in the long term, returning to baseline sleep and activity levels within 24 hours (Figure 1- figure supplement 3A, B). Second, both $A\beta^{short}$ and $A\beta^{long}$ injected larvae responded normally to salient stimuli such as a light:dark pulse, demonstrating that these larvae were not paralyzed, in a coma, or undergoing sickness behavior (Figure 1- figure supplement 3C). Finally, we considered if the changes in motility in Aβ-injected larvae were seizure-like behaviors. Wild type (WT) zebrafish larvae display “burst-and-glide” movements characterized by single short forward or turn movement followed by a short pause (Figure 1- figure supplement 3D and Figure 1- video 1). In

contrast, epileptogenic drugs like the GABA-receptor antagonist PTZ induce electrophysiological and behavioural seizures (Baraban et al, 2005), which are observed as dramatic rearrangements in zebrafish bout structure (Figure 1-figure supplement D). The bout structure of $A\beta^{rev}$, $A\beta^{short}$, and $A\beta^{long}$ injected fish was highly similar to WT behavior (Figure 1-figure supplement 3D, E and Figure 1- video 1), and the high frequency bouts (HFB) indicative of seizures (Reichert et al., 2019) were only found in PTZ exposed fish but not Aβ injected larvae (Figure 1- figure supplement 3D, E). Together these experiments indicate that exposure to Aβ modulates normal sleep/wake behaviour without inducing toxic states.

We conclude that the changes in behavior after Aβ exposure are due to acute signalling events and therefore sought to identify the neuronal and molecular substrates through which Aβ signals to modulate sleep/wake behavior.

$A\beta^{short}$ and $A\beta^{long}$ induce opposing changes in neuronal activity and differentially engage sleep-promoting neurons

If Aβ oligomers alter behavior through acute signalling in the brain, the differential effects of $A\beta^{short}$ and $A\beta^{long}$ should be reflected at the level of neuronal activity. In situ hybridization (ISH) for expression of the immediate early gene, *c-fos*, identified several discrete areas of the larval brain that are upregulated after injection of $A\beta^{short}$ relative to $A\beta^{rev}$, including the posterior hypothalamus and the dorsal and ventral telencephalon (Figure 2A). Comparing the $A\beta^{short}$ induced *c-fos* patterns to WT brains collected at zeitgeber time 1 (ZT1, ZT0=lights ON), when larvae are maximally awake, reveals at least 9 populations of *c-fos* positive neurons in both $A\beta^{short}$ and waking brains (Figure 2A, C). In contrast, *c-fos* expression following $A\beta^{long}$ injections

was globally dampened relative to $A\beta^{rev}$ (Figure 2B) in a manner consistent with the low expression of *c-fos* in WT brains collected at ZT19, when larvae are maximally asleep (Figure 2C).

Immediate early gene expression is an imperfect readout of changes in neuronal activity and brain state, as baseline *c-fos* is expressed in low amounts in zebrafish and has a relatively slow time course of 15-30 minutes for transcription of mRNA (Baraban et al., 2005). We therefore also quantified changes in the more rapid (<5 minutes) neuronal activity marker, phosphorylated ERK (p-ERK), using the larval zebrafish MAP-Mapping technique (Randlett et al., 2015). This method identifies the relative quantitative changes in brain region-specific levels of p-ERK relative to total ERK between Aβ injections and reverse peptide control conditions. Consistent with *c-fos* induction, $A\beta^{short}$ upregulated P-ERK in the ventral telencephalon and posterior hypothalamus (Figures 2D and 2D', Figure 2-source data 1), while $A\beta^{long}$ resulted in a widespread reduction in p-ERK levels throughout most of the brain (Figures 2E and 2E', Figure 2-source data 2). These brain activity states are consistent with the induction of wakefulness by $A\beta^{short}$ and sleep by $A\beta^{long}$.

Finally, if the behavioral states induced by Aβ are bona fide sleep/wake states, we reasoned that known zebrafish sleep/wake regulatory neurons should be engaged. Galanin-expressing neurons of the preoptic area and hypothalamus are active and upregulate *galanin* transcription during zebrafish sleep (Reichert et al, 2019). Similarly, ISH for galanin 4-6 hours post-injection of Aβ oligomers revealed that wake-promoting $A\beta^{short}$ slightly decreased (-6%, blinded counts), while sleep-promoting $A\beta^{long}$ slightly increased (+12%, blinded counts), the number of *galanin* positive

cells in the hypothalamus compared to $A\beta^{rev}$ injected larvae (Figure 2F-G). The differential effects on *galanin* neurons are consistent with that the induction of wakefulness by $A\beta^{short}$ and sleep by $A\beta^{long}$.

Aβ binding targets are required for behavioral responses to Aβ

Many candidate Aβ binding partners have been implicated in mediating the signalling effects of Aβ on synapses, with some targets showing preferences for Aβ dimers, such as Adrenergic Receptor β2 (ADRB2) (Wang et al., 2010), or low molecular weight (50-75 kDa) species, such as the Progesterone Membrane Receptor Component 1 (PGRMC1) (Izzo et al., 2014b), while other targets preferentially bind to longer oligomers/protofibrils, such as the Prion Protein (PrP) (Lauren et al., 2009; Nicoll et al., 2013). We therefore used Crispr/Cas9 to make genetic lesions in several zebrafish candidate Aβ receptors, choosing examples with reported affinities for various sized Aβ oligomers (Figures 3- figure supplement 1 and Figure 4 – figure supplement 1). We isolated a *pgrmc1* allele with a 16 bp deletion that leads to a frameshift and early stop codon that truncates the protein before a conserved Cytochrome b5-like Heme/Steroid binding domain (Figure 3- figure supplement 1A-D). We also isolated an *adrb2a* allele with an 8bp deletion that leads to a severely truncated protein lacking all transmembrane domains (Figure 3- figure supplement 1E-G). We also obtained a $prp1^{-/-};prp2^{-/-}$ double mutant (Fleisch et al., 2013; Leighton et al., 2018) that lacks both zebrafish Prp proteins with conserved Aβ binding sites (Figure 4 -figure supplement 1). The third zebrafish *prion* gene product, Prp3, does not have the conserved Aβ binding domains present in Prp1 and Prp2 (Figure 4 -figure supplement 1). Except for a mild increase in daytime sleep in $adrb2a^{-/-}$ mutants (Figure 3 -figure supplement 2D'-F'), none of these mutants exhibited changes in baseline sleep and wake on a 14hr:10hr light:dark

cycle as compared to wild type and heterozygous siblings (Figures 3- figure supplement 2A-F'; Figures 4- figure supplement 2A-F'). Under baseline conditions, we also detected no significant differences in day or night sleep and waking activity in *prp* double mutants compared to $prp^{+/+}$ siblings generated from either $prp1^{+/-}; prp2^{+/-}$ or $prp1^{+/-};prp2^{-/-}$ in-crosses (Figure 4- figure supplement 2A-F'). The mild baseline phenotypes allowed us to test the effect of Aβ oligomers in these mutants without complex behavioral confounds.

We first tested the effects of $A\beta^{short}$ injection on mutant behavior. Unlike the wild type controls, neither the $adrb2a^{-/-}$ nor the $pgrmc1^{-/-}$ mutants increased waking activity (Figures 3A-3C and 3E) or suppressed sleep as observed in wild type controls (Figures 3A'-3C' and 3G). Injection of $A\beta^{short}$ into $adrb2a^{-/-}$ animals even significantly increased sleep (+83.7%) instead of reducing it as in wild type larvae (Figures 3B' and 3G). In contrast, $A\beta^{short}$ injected into mutants that lack both zebrafish Prp orthologs ($prp1^{-/-}; prp2^{-/-}$) elicited slightly stronger increases in waking activity and significantly large (-45%) reductions in sleep (Figures 3D, D', F and H). Thus, the wake-promoting activity of $A\beta^{short}$ requires intact Adrb2a and Pgrmc1 but not functional Prp1 and Prp2.

Because the size of oligomeric species in our $A\beta^{long}$ preparation (20-400 nm) falls into the size range that exhibits high-affinity binding to mammalian Prion Protein (PrP) (20-200 nm) and thereby acts to modulate synapses (Gimbel et al., 2010; Lauren et al., 2009; Nicoll et al., 2013; Um et al., 2012), we tested whether PrP is instead required for $A\beta^{long}$-induced sleep. After injection of $A\beta^{long}$, $prp1^{-/-};prp2^{-/-}$ null mutants failed to increase sleep compared to wild type controls (Figures 4A-D). The modest reduction of wakefulness induced by $A\beta^{long}$ was even

reversed in *prp1*$^{-/-}$*;prp2*$^{-/-}$ mutants, with Aβ^{long} instead significantly increasing wakefulness (Figure 4C). Thus, while Prps are not required for the wake-inducing effects of Aβ^{short}, functional Prp1 and Prp2 are essential for sleep induced by Aβ^{long}. Moreover, since *prp* double mutants have exacerbated wakefulness in response to Aβ^{short} injections, the sleep-inducing Prp pathway is likely co-activated along with the wake-promoting pathway by Aβ to partially dampen the behavioral response of wild type larvae (Figure 3D and 3H).

Mutants lacking Aβ targets have altered brain activity in response to Aβ consistent with behavioral effects

If Aβ^{short} interacts with Adrb2a and Pgrmc1 to drive changes in wakefulness, the increased neuronal activity we observed in wild type larvae after Aβ^{short} injections (Figure 2A) should also be abolished in the *adrb2a*$^{-/-}$ and *pgrmc1*$^{-/-}$ mutant backgrounds. Consistently, lack of either Adrb2a or Pgrmc1 abolished the neuronal activity-inducing effect of Aβ^{short} (Figure 5A), as detected by in situ hybridization for *c-fos***.** In particular, the neuronal activity observed in the posterior hypothalamus and the dorsal and ventral telencephalon after Aβ^{short} into WT controls was not detected after injection into either *adrb2a*$^{-/-}$ or *pgrmc1*$^{-/-}$ mutants (Figure 5A). This result is consistent with Aβ^{short} failing to induce wakefulness in these mutants. Similarly, although Aβ^{long} dampens neuronal activity when injected into wild type larvae, Aβ^{long} injections into the *prp1*$^{-/-}$*; prp2*$^{-/-}$ double mutants elicited no reduction in *c-fos* expression (Figure 5B). Instead, *c-fos* expression in the telencephalon and hypothalamus was upregulated relative to reverse injected controls (Figure 5B), consistent with the increased behavioral wakefulness observed in the *prp* mutants (Figure 4C). Together, these data are consistent with Aβ^{short} acutely upregulating neuronal activity and behavioral wakefulness through interactions with Adrb2a and Pgrmc1,

while $A\beta^{long}$ interactions with Prp drive increased sleep and a global reduction in neuronal activity.

Pharmacological blockade of the Prp-mGluR5-Fyn kinase signalling cascade prevents sleep induction by $A\beta^{long}$

One of the advantages of using the zebrafish model system is the ability to perturb Aβ signalling cascades with small molecule inhibitors added directly to the water (Kokel et al., 2010; Rihel et al., 2010). To further dissect the $A\beta^{long}$-PrP sleep-inducing pathway, we focused on disrupting the putative signalling cascade downstream of Aβ-Prp interactions that lead to synaptic changes in neuronal culture (Um et al., 2012) (Figure 6A). Consistent with a role for direct $A\beta^{long}$-Prp interactions in sleep, soaking the larvae in Chicago Sky Blue 6B, a small molecule reported to disrupt Aβ-PrP interactions (Risse et al., 2015), significantly abolished the sleep-inducing effect of $A\beta^{long}$ (Figures 6B, 6C, S7A and Figure 6-figure supplement 1A,B). Similarly, pharmacological inhibition of either of the putative Aβ-Prp downstream signalling components Metabotropic Glutamate Receptor 5 (mGluR5) or Fyn kinase (Um et al., 2013; Um et al., 2012) significantly blocked the sleep-inducing properties of $A\beta^{long}$ (Figures 6D, 6E, Figure 6- figure supplement 1C, D). Both the mGluR5 inhibitor MPEP and the Src-kinase inhibitor saracatinib even resulted in significant sleep reductions after exposure to $A\beta^{long}$. Overall, these results are consistent with the effect of genetic ablation of *prp1* and *prp2*. Thus, both genetic and pharmacological interference with several steps of the Aβ-Prp-mGluR5-Fyn kinase signalling cascade prevents the ability of $A\beta^{long}$ to increase sleep behavior.

$A\beta^{short}$ and $A\beta^{long}$ affect sleep through distinct neuronal/molecular pathways

Although long and short oligomers require different receptors to affect behavior, they may act within the same neuronal circuit signalling cascade. If so, one phenotype should predominate over the other when the two oligomers are co-administered. Alternatively, oligomers may signal through parallel signalling circuits to bi-directionally modulate sleep in an additive manner. To test this, we co-injected $A\beta^{short}$ and $A\beta^{long}$ in a 1:1 ratio and compared the sleep phenotype to injection of either oligomer alone. As expected, $A\beta^{short}$ alone reduced sleep and $A\beta^{long}$ alone increased sleep. In contrast, co-injection of both $A\beta^{short}$ and $A\beta^{long}$ resulted in an intermediate phenotype that is indistinguishable from control injections of $A\beta^{rev}$ (Figure 6F), suggesting that the effects of $A\beta^{short}$ and $A\beta^{long}$ are additive and likely act through distinct neuronal circuits or signalling cascades to modulate sleep.

Considering this result is aligned with the genetic and pharmacological data, we propose a bi-directional model of Aβ sleep regulation in which $A\beta^{short}$ and $A\beta^{long}$ act through distinct receptors and neuronal pathways to independently modulate behavioral state (Figure 6G). In this model, the presence of both oligomers leads a balance of signalling through sleep-promoting and sleep-inhibiting pathways, resulting in little or no change in behaviour. Tipping the balance from one oligomeric state to the other leads to either the sleep activating or the sleep inhibiting pathway to predominate.

DISCUSSION

Previous studies have suggested that changes in sleep during AD may further accelerate Aβ accumulation and neuronal damage, creating a vicious cycle that leads to further neuronal dysregulation and increased sleep-wake cycle abnormalities (Roh et al., 2012). Our results show

that, depending on its oligomeric form, Aβ can acutely increase or decrease sleep and wake behaviors and brain states through behaviorally relevant molecular targets and independently of neuronal cell death. The exogenous application of Aβ oligomers in our experiments limit the conclusions we can draw about endogenous functions of Aβ, which *in vivo* may present with different structure, local concentrations, and kinetics. However, the bi-directional Aβ modulation of sleep and wakefulness (Figure 6G) predicts that alterations to the relative concentrations of different Aβ oligomeric forms during healthy aging and AD disease progression will have opposing consequences on sleep and wake behavior.

Distinct molecular pathways for Aβ sleep-wake regulation

We found that $A\beta^{short}$-triggered wakefulness required intact Adrb2a and Pgrmc1, while $A\beta^{long}$-induced sleep required functional Prp signalling. These data are consistent with a model in which Aβ directly binds to these targets to modulate downstream signalling cascades that ultimately affect neuronal circuits that regulate behavioral state. Our results match well with previous reports demonstrating binding preferences of Aβ dimers, trimers, and 56kDa oligomers for different targets *in vitro*. For example, Aβ dimers, which have been detected in the brains of AD patients (Vazquez de la Torre et al., 2018), have been shown to directly bind human ADRB2 with high-affinity, causing increased calcium influx and neuronal hyper-activation in rat prefrontal cortical slices (Wang et al., 2010). PGRMC1 can be activated by AD brain extracts (Izzo et al., 2014b) and also has shown preferential binding for 50-75 kDa Aβ species *in vitro* (Izzo et al., 2014a). Both types of shorter Aβ species that bind to ADRB2 and PGRMC1 fall within the size ranges that induce Adrb2a- and Pgrmc1-dependent wakefulness in zebrafish larvae. Our results are also consistent with studies that have identified PrP as a direct binding

partner (Lauren et al., 2009) for longer Aβ-oligomers of 20-200 nm in length (Nicoll et al., 2013), the size range of our sleep-inducing $A\beta^{long}$ preparation. In neuronal culture and slice preparations, longer Aβ-oligomers trigger reduction of synaptic strength (Lauren et al., 2009) via a Prp signalling cascade through mGluR5 and Fyn kinase activation (Um et al., 2012). Similarly, we found that pharmacological blockade of either the direct Aβ-Prp interaction (with Chicago Sky Blue), mGluR5 signalling (with MPEP), Fyn kinase activity (with saracatinib), or by mutation of the Prp receptors prevented the widespread reduction of neuronal activity and increase in sleep that was induced by longer Aβ-oligomers.

Although triggering neuronal and behavioral changes through distinct molecular pathways, several aspects of Aβ's effects on sleep-wake regulation remain to be elucidated. For example, the elimination of either Adrb2a or Pgrmc1 is sufficient to fully prevent $A\beta^{short}$-induced wakefulness. This suggests that Adrb2a and Pgrmc1 function in the same molecular pathway, and signalling by Aβ on either alone is insufficient to modulate behavior. Not much is known about how these two receptors interact with one another, but at least one study (Roy et al., 2013) has suggested they can directly physically interact. Whether $A\beta^{short}$ binds both receptors to affect behavior or whether one receptor is an obligate component of the other's ability to transmit Aβ signals is currently unclear. It also remains unclear if the $A\beta^{short}$-Adrb2a/Pgrmc1wake pathway and the $A\beta^{long}$-Prp sleep pathway occur in the same or different sets of neurons to modulate behavior, as these receptors have widespread expression in zebrafish (Cotto et al., 2005; Malaga-Trillo et al., 2009; Steele et al., 2011; Thisse, 2004; Wang et al., 2009), although our co-injection experiment suggests they act on parallel neuronal circuits. Numerous wake- and sleep-promoting neuronal populations that could serve as neuronal targets for these signalling cascades to drive

changes in behavioral state have been uncovered in zebrafish (Barlow and Rihel, 2017). Future experiments will be needed to tease out the neuronal components involved, for example by replacing functional receptors into candidate neurons in otherwise mutant animals and rescuing the responses to Aβ, or by mutating receptors selectively in cell types with conditional genetics.

Altered Aβ oligomeric ratio—implications for sleep in health and AD

Our model investigates alterations in sleep/wake behavior due to acute changes in exogenously delivered Aβ levels. Thus, it is possible that the sleep/wake effects observed in our study may be different than those observed when Aβ fluctuates over 24hr or when it is chronically accumulating as in AD. However, our model predicts that alterations to the ratio of Aβ oligomeric forms present in the brain could have differential effects on sleep-wake regulation, as the balance between sleep- and wake- promoting Aβ signals is tilted to favour one pathway over the other (Figure 6G).

Given the natural daily increase in Aβ secretion during wakefulness and increased levels of Aβ clearance during sleep (Xie et al., 2013), changes in extracellular Aβ levels could sculpt behavior over the normal 24-hr circadian cycle. As Aβ burden is acutely increased by sleep deprivation (Shokri-Kojori et al., 2018), perturbations to the normal sleep-wake cycle may feedback on behavior through altered Aβ signalling. Other phenomena have been reported to alter Aβ generation and fibrilization over short time-scales. For example, temperature changes in the physiological range (35-42°C) have been reported to significantly affect Aβ oligomerization (Ghavami et al., 2013), suggesting that either the natural daily fluctuation in body temperature (in humans, up to 2°C) or the induction of a fever can promote changes in amyloidogenic Aβ

410 generation (Szaruga et al., 2017). In addition, Aβ can act as an antimicrobial peptide (Kumar et
411 al., 2016; Soscia et al., 2010), and microbial infection can trigger Aβ fibrilization (Eimer et al.,
412 2018). Considering that infection and fever are also potent drivers of sleep (Imeri and Opp,
413 2009), the sleep-inducing Aβ-Prp signalling pathway we identified here could mediate recovery
414 sleep during illness-- a hypothesis for future investigation.
415
416 On longer timescales, the amount and type of Aβ oligomeric species (including dimers, cross-
417 linked dimers, trimers, and 56 kDa oligomers) found in healthy brains change across the human
418 life cycle (Lesne et al., 2013) and are heterogeneous and elevated in AD patients (Izzo et al.,
419 2014a; Kostylev et al., 2015). Although the precise makeup of Aβ species present in healthy and
420 AD brains has remained difficult to quantify (Benilova et al., 2012), some studies have indicated
421 that short (dimers, trimers) Aβ oligomers are more enriched in the early, mild cognitive
422 impairment (MCI) stages of AD, while longer oligomers predominate in the CSF at later clinical
423 stages of AD (De et al., 2019). Similarly, AD progression is associated with increasingly large
424 disruptions in sleep patterns, with patients exhibiting high levels of sleep fragmentation, a lack of
425 circadian rhythm, night-time insomnia and irregular daytime napping throughout the day
426 (Videnovic et al., 2014). One possibility consistent with our data is that sleep symptoms of both
427 normal aging and AD may reflect changes in Aβ burden that lead to an altered balance in sleep-
428 and wake-promoting signalling cascades. These signalling molecules might therefore be
429 potential therapeutic targets for treating disrupted sleep early in AD progression, which may in
430 turn slow disease progression.
431
432 **Acknowledgments:**

We thank Tom Hawkins and Mark Turmaine for assistance with TEM, Gaia Gestri for assistance with heart injections and Marcus Ghosh for assistance with tERK/pERK experiments. We also thank Dervis Salih, Steve Wilson, and John Hardy for their comments and all first-floor fish lab members for their input throughout the project.

Funding: This was supported by operating funds to WTA from the Alzheimer Society of Alberta & Northwest Territories and Alberta Prion Research Institute of Alberta Innovates. PLAL was supported by Alzheimer Society of Canada, and JR was funded by an Interdisciplinary Research Grant from the Alzheimer's Research UK, an ERC Starting Grant (#282027), a Wellcome Trust Investigator Award (#217150/Z/19/Z), and a UCL Excellence Fellowship.

Author Contributions: GGO and JR conceived and designed the experiments. GGO performed all experiments with assistance from SL. GGO, JR, and SL analysed the data. GGO and SL generated the *adrb2a* and *pgrmc1* mutants. PLAL and WTA generated the *prp1* and *prp2* mutants. GGO and JR wrote the manuscript with input from all authors. JR supervised the project.

Declaration of interests: The authors declare no competing interests.

Data and materials availability: All data is available in the manuscript or the supplementary materials.

List of Supplementary Materials:

Materials and Methods

Key Resource Table

454 7 figure supplements

455 2 source data

456 1 video

457

458

459 **Figure Legends**

460 **Figure 1**. **Aβ oligomers bi-directionally affect sleep and wake in zebrafish larvae.**

461 A) Experimental schematic. Aβ was injected into the heart of 5 dpf larvae in the morning (ZT2=
462 zeitgeber time 2, i.e. 2hr after lights on). Behavior was then monitored in a square-welled 96-
463 well plate for 24-48 hrs on a 14hr:10hr light:dark cycle.

464 B) Heart-injected HiLyteTM Fluor 647-labeled Aβ42 (fAβ) penetrated the whole larval brain as
465 visualized by confocal microscopy (optical sections, dorsal view) taken 2 hr after injection.
466 Anterior is to the top.

467 C) Aβ prepared under increasing temperatures adopted longer oligomeric lengths, as measured
468 by transmission electron microscopy. Each dot is a single oligomer (N=number measured), and
469 the bars show the median. Data was taken from five randomly selected micrographs from two
470 independent experiments. **$p \leq 0.01$, ****$p \leq 1x10^{-7}$ Kruskal-Wallis, Tukey-Kramer post-hoc
471 test.

D, E) Exemplar 24-hr traces post-injection comparing the effect of $A\beta^{short}$ (blue) on average waking activity (D) and sleep (E) versus $A\beta^{rev}$ controls (grey). Ribbons represent ± the standard error of the mean (SEM). Light and dark bars indicate the lights ON and lights OFF periods, respectively. N= the number of larvae in each condition.

D', E') The effect of $A\beta^{short}$ relative to $A\beta^{rev}$ on waking (D') and sleep (E') during the first day is shown, pooled from n=5 independent experiments. Each dot represents a single larva normalized to the mean of the $A\beta^{rev}$ control, and error bars indicate ± SEM. The mean difference effect size and 95% confidence interval is plotted to the right. *p<0.05, ^{T}p<0.1, one-way ANOVA.

F, G) Exemplar 24-hr traces post-injection comparing the effect of $A\beta^{long}$ (green) on average waking activity (F) and sleep (G) versus $A\beta^{rev}$ controls (grey).

F', G') The effect of $A\beta^{long}$ relative to $A\beta^{rev}$ on waking (F') and sleep (G') during the first day is shown, pooled from n=4 independent experiments. *p<0.05, **p<0.01, one-way ANOVA.

H, I) Exemplar 24-hr traces post-injection comparing the effect of $A\beta^{v\_long}$ (magenta) on average waking activity (H) and sleep (I) versus Aβ reverse peptide controls (grey).

H', I') The effect of $A\beta^{v\_long}$ relative to $A\beta^{rev}$ on waking (H') and sleep (I') during the first day is shown, pooled from n=3 independent experiments.

J) The effect of different Aβ preparations on the number of sleep bouts relative to $A\beta^{rev}$ controls. The difference effect size and 95% confidence interval is plotted below. The asterisks indicate statistically significant different effects among the preps (***p<0.001, one-way ANOVA).

See also Figure 1-figure supplement 1-3.

Figure 2. Aβ oligomers differentially alter neuronal activity in the larval zebrafish brain.

A) As detected by ISH, the immediate early gene *c-fos* is upregulated in many larval brain areas following $A\beta^{short}$ injection, including the dorsal and ventral telencephalon (tel) and the posterior hypothalamus (black arrowheads), relative to Aβ reverse control injections. Other upregulated areas in the midbrain and hindbrain are indicated (white arrowheads). hyp- hypothalamus; hb- hindbrain. D=dorsal, P=Posterior, R=Right. n=blind counts of brains with the shown expression pattern/total brains. 24/43 stringently counts only brains with the major areas upregulated.

B) Compared to $A\beta^{rev}$ injections, $A\beta^{long}$ oligomers induce less *c-fos* expression. The $A\beta^{rev}$ and $A\beta^{long}$ treated brains were stained longer than in panel A) to ensure detection of weaker *c-fos* expression. n =blind counts of number of brains with the shown expression /total brains.

C) *c-fos* is upregulated in many larval brain areas at 10 am (ZT1) awake fish, including the dorsal and ventral telencephalon and the posterior hypothalamus (black arrowheads), and other discrete regions of the mid and hindbrain (white arrowheads). *c-fos* expression is downregulated in later timepoints (ZT13) and is very low in ZT19 brains, when larvae are predominantly asleep. N=10 fish/ timepoint.

D, D') Brain expression of the neuronal activity correlate pERK/tERK comparing $A\beta^{short}$ (n =6) to $A\beta^{rev}$ (n = 5) injected larvae identified areas upregulated (green) and downregulated (magenta) by $A\beta^{short}$. Data are shown as a thresholded maximum projection overlaid on the Z-Brain Atlas tERK reference (gray). White arrowheads indicate regions in the ventral telencephalon and

posterior hypothalamus that are upregulated similar to *c-fos* in A). Dorsal view in D), lateral view in D').

E, E') pERK/tERK expression after $A\beta^{long}$ injections (n=7) shows widespread downregulation of neuronal activity (magenta) compared to $A\beta^{rev}$ controls (n=7), consistent with *c-fos* data in B. Dorsal view in E), lateral view in E').

F) As detected by ISH, the number and intensity of hypothalamic *galanin* positive neurons are downregulated following $A\beta^{short}$ injection and upregulated following $A\beta^{long}$ injection, relative to Aβ reverse control injections. Representative images from N=22-24 per condition.

G) Normalized, blinded counts of hypothalamic *galanin*-positive cell numbers 4-6 hours after $A\beta^{short}$ and $A\beta^{long}$ injections, relative to $A\beta^{rev}$. Error bars indicate ± SEM. The mean difference effect size and 95% confidence interval is plotted at the bottom. **p<0.01, one-way ANOVA.

See also Figure 2-source data 1 and 2.

Figure 3. Wake induction by $A\beta^{short}$ requires Adrb2a and Pgrmc1, but not the Prion Protein.

A-D') Exemplar 24-hr traces comparing the effects of $A\beta^{short}$ oligomers on average waking activity (A-D) and sleep (A'-D') versus $A\beta^{rev}$ injected into wild type (A,A'), *adrb2a*$^{-/-}$ (B,B'), *pgrmc1*$^{-/-}$ (C,C'), and *prp1*$^{-/-}$;*prp2*$^{-/-}$ mutants (D,D').

E-H) The effect of $A\beta^{short}$ relative to $A\beta^{rev}$ on normalized waking activity (E and F) and sleep (G and H) during the first day is shown. Each dot represents a single larva normalized to the mean of the $A\beta^{rev}$ control, and error bars indicate ± SEM. The mean difference effect size and 95% confidence interval are plotted below. N= the number of larvae. The wake inducing and sleep suppressing effects of $A\beta^{short}$ are absent in (E,G) *adrb2a*$^{-/-}$ and *pgrmc1*$^{-/-}$ but enhanced in *prp1*$^{-/-}$;*prp2*$^{-/-}$ mutants (F,H). $^{ns}p>0.05$, $^{*}p\leq0.05$, $^{**}p\leq0.01$, $^{***}p\leq0.0001$, $^{****}p\leq10^{-5}$ one-way ANOVA. Data is pooled from n=2 independent experiments for *adrb2a*$^{-/-}$ and *pgrmc1*$^{-/-}$ and n=3 for *prp1*$^{-/-}$;*prp2*$^{-/-}$.

See also Figure 3- figure supplement 1 and 2.

Figure 4. Sleep induction by $A\beta^{long}$ requires signalling through Prion Protein

A-B') Exemplar 24-hr traces comparing the effects of $A\beta^{long}$ oligomers on average waking activity (A,B) and sleep (A'-B') versus $A\beta^{rev}$ on wild type (A,A'), and *prp1*$^{-/-}$;*prp2*$^{-/-}$ mutant (B,B') backgrounds.

C-D) The effect of $A\beta^{long}$ relative to $A\beta^{rev}$ on normalized waking (C) and sleep (D) on wild type and *prp1*$^{-/-}$;*prp2*$^{-/-}$ mutant backgrounds (mixed *prp3* background) during the first day is shown. The activity reducing (C) and sleep promoting (D) effects of $A\beta^{long}$ are blocked in *prp1*$^{-/-}$;*prp2*$^{-/-}$ mutants. $^{**}p\leq0.01$, $^{****}p\leq10^{-5}$ one-way ANOVA. Data is pooled from n=3 independent experiments.

549 See also Figure 4- figure supplement 1 and 2.

550

551 **Figure 5. Neuronal activity after exposure to Aβ preparations is altered in mutants of Aβ**
552 **binding targets**

553 A) After $A\beta^{short}$ injection into WT larvae (top right), *c-fos* is detected in many larval brain areas,
554 including the dorsal and ventral telencephalon and posterior hypothalamus (black arrowheads),
555 but not after injection of Aβ reverse controls (left). In contrast, $A\beta^{short}$ injections into either
556 *adrb2a*$^{-/-}$ (middle right) or *pgrmc1*$^{-/-}$ mutants do not induce *c-fos* expression. The brains in the
557 middle and lower panels were stained longer than the WT (+/+) brains to ensure detection of
558 weaker expression. D=dorsal, P=Posterior. n =blinded counts of brains with expression pattern/
559 total brains.

560 B) Compared to $A\beta^{rev}$ injections, $A\beta^{long}$ oligomers induce less *c-fos* expression in WT larvae (top
561 panels). In contrast, $A\beta^{long}$ induced relatively increased *c-fos* expression in the telencephalon and
562 posterior hypothalamus (black arrows) in the *prp1*$^{-/-}$, *prp2* $^{-/-}$ double mutants. These $A\beta^{rev}$ and
563 $A\beta^{long}$ treated brains were stained longer to ensure detection of weaker *c-fos* expression.
564 D=dorsal, P=Posterior.

565 **Figure 6. Pharmacological blockade of the $A\beta^{long}$-Prp-mGluR5-Fyn Kinase signalling**
566 **cascade prevents increases in sleep.**

A) Schematic showing how Aβ–Prp interactions signal through mGluR5 to activate Fyn kinase, leading to synaptic changes (Nygaard et al., 2014). Small molecules that block each step in the pathway are indicated.

B) Representative traces of sleep behavior after $A\beta^{long}$ versus $A\beta^{rev}$ injections in the absence (left) or presence (right) of the Aβ-Prion binding disruptor, Chicago Sky Blue (3nM). Ribbons represent ± SEM.

C) The effect of $A\beta^{long}$ relative to $A\beta^{rev}$ on normalized sleep during the first day in the in the absence or presence of 3nM Chicago Sky Blue. The data is pooled from n= 2 independent experiments **$p \leq 0.01$, one-way ANOVA.

D) Representative traces of sleep behavior after $A\beta^{long}$ versus $A\beta^{rev}$ injections in the presence of mGluR5 inhibitor MPEP (5uM, left) and Fyn Kinase inhibitor saracatinib (300 nM, right). Ribbons represent ± SEM.

E) The effect of $A\beta^{long}$ relative to $A\beta^{rev}$ on normalized sleep during the first day in the absence or presence of 5 uM MPEP (left) and 300 nM saracatinib (right). Each dot represents a single larva normalized to the mean $A\beta^{rev}$. Data is pooled from 2 independent experiments. **$p \leq 0.01$, ****$p \leq 10^{-5}$ one-way ANOVA.

F) The effect of a 1:1 mixture of $A\beta^{long}$ to $A\beta^{short}$ relative to single injections of $A\beta^{rev}$, $A\beta^{short}$, and $A\beta^{long}$ on normalized sleep during the first day. The data is pooled from n= 4 independent experiments.

G) A bi-directional model for sleep/wake regulation by Aβ. In wild type animals (centre), injection of $A\beta^{short}$ species signal through Adrb2a/Pgrmc1 to drive wakefulness while $A\beta^{long}$ oligomers signal via Prp to induce sleep. In mutants that lack Prp (left), only $A\beta^{short}$ species (as shown by the overlapping distributions) remain to inhibit sleep with no residual $A\beta^{long}$ oligomers to stimulate the sleep-inducing pathway to counteract wake-inducing signals. Thus *prp1*$^{-/-}$*; prp2*$^{-/-}$ mutants have enhanced wakefulness in response to Aβ. Conversely, mutants that lack Adrb2a/Pgrmc1 (right), retain only the sleep-promoting Aβ pathway and fail to increase wakefulness in response to $A\beta^{short}$.

See also Figure 6- figure supplement 1.

Materials and Methods

See the Key Resource Table (Supplementary File 1: Key Resources Table) for details of reagents.

Zebrafish strains and husbandry

Zebrafish (Danio rerio) were raised under standard conditions at 28°C in a 14:10 light:dark cycle and all zebrafish experiments and husbandry followed standard protocols of the UCL Zebrafish Facility. AB, TL and ABxTup wild-type strains were used in this study. *prp1* (ua5003/ua5003), *prp2* (ua5001/5001), *adrb2a (*u511/u511) and *pgrmc1 (*u512/u512*)* mutants were outcrossed multiple times and *pgrmc1* F2 and *adrb2a* F2 generations were used for behavior. Ethical approval for zebrafish experiments was obtained from the Home Office UK under the Animal Scientific Procedures Act 1986 with Project licence numbers 70/7612 and PA8D4D0E5 to JR.

Aβ preparations

HFIP treated Aβ42 peptide (JPT Peptide Technologies) and Aβ42-1 reversed peptide (Sigma) were dissolved in DMSO, vortexed occasionally for 12 min at room temperature and sonicated for 5 min to obtain 100 µM solution. The stock solutions were aliquoted as 5 µl in individual tubes and are kept are -80^{o}C. 1 µl of the 100 µM stock was diluted in (Phosphate buffered saline) PBS to yield 10 µM solutions which were incubated at 4°C, 25°C or 37°C for 24 hours (Kusumoto et al., 1998; Orban et al., 2010; Whitcomb et al., 2015). 1 hour before injecting, this stock was diluted to 10 nM using 1:10 serial dilutions in PBS and kept at the respective temperature (4^{o}C, 25^{o}C, 37^{o}C) until injecting.

Transmission Electron Microscopy (TEM)

1 µl of (4^{o}C, 25^{o}C or 37^{o}C incubated) 10 µM Aβ solution was loaded onto formvar/carbon coated 300 mesh grids from Agar Scientific. The grid was washed twice in 20 mM phosphate buffer for 10 seconds and negatively stained in 2% aqueous uranyl acetate for 30 seconds. After drying for 2-3 days, samples were imaged using a Phillips TEM. At least 5 micrographs were used for each condition to blindly measure the length of the Aβ42 oligomeric structures using at least 30 measurements/condition. Using FIJI, 30-50 measurements were taken for each condition by drawing a free-hand line on the fibril, which was then scaled using the scale bar.

Heart injections

Injections were carried out blindly with a Pneumatic PicoPump (WPI) and glass capillary needles (Science Products Gmbh) prepared with a Micropipette Puller (Shutter Instruments). 5 dpf larvae were anesthetized using 4%Tricaine (42 mg/L, Sigma) 30 min before injections.

633 Larvae were immobilized in 1.8 % low melting point agarose (ThermoFischer) in fish water on
634 their sides on a slide. 1 nL of Aβ (10 nM starting concentration) was injected into the heart
635 chamber of the fish along with a high molecular weight fluorescent dye (2000 kDa dextran-
636 conjugated FITC (3 mg/ml, Sigma). We estimate that 1 nl of a 10 nM Aβ injection into a ~3.01
637 (±0.16) x10^8 μm^3 (285-317 nL) 5dpf larva[43] yields a final monomeric brain/CSF concentration of
638 ~28-32 pM. The success of the injection was checked under a standard fluorescent scope by the
639 presence of fluorescence in the heart of the animal. Larvae were transferred to fresh fish water
640 for 20 min to recover from Tricaine and transferred to sleep/wake behavior box. For drug
641 blocking experiments, zebrafish larvae were soaked into 3 nM Chicago Sky Blue 6B (Sigma), 5
642 µM MPEP (Cambridge Biosciences), 300 nM Saracatinib (Generon) 1 day before the injections
643 (from 4-5 dpf). Fluorescently tagged HiLyte™ Fluor 647-labeled Aβ42 (Eurogentech LTD) was
644 injected at 10 µM.
645

646 *Behavioral experiments*
647 Larval zebrafish behavioral experiments were performed and analysed as described (Rihel et al.,
648 2010). Briefly, 5 dpf larvae were transferred to 96 square-well plates and continuously
649 illuminated with IR and white lights from 9 am to 11 pm in a Zebrabox (Viewpoint life sciences)
650 for 24-48 hours. The movement of each larva was measured and duration of movement was
651 recorded with an integration time of 10 sec. Data were processed according to Rihel et al.,
652 (2010), and statistical tests were performed using MATLAB. Mutant larval zebrafish
653 experiments were performed on siblings from heterozygous in-crosses, differing only in the
654 mutation of the specific gene and genotyped at the end of the experiment.

Dark Pulse Experiments:

Larvae are placed in the behavior tracking boxes, 2 or 3 dark pulses for 10 minutes with a 2-4 hour interval were introduced in four independent experiments. For data analysis, only the dark pulses after the acclimatization period in the late afternoon were combined for each genotype.

In situ hybridization

RNA in situ hybridization (ISH) to detect *c-fos* and galanin was performed as described (Thisse and Thisse, 2008). Zebrafish larvae were fixed in 4% paraformaldehyde in PBS at 4°C overnight. A template for *in vitro* transcription was generated by PCR using a reverse primer that contains a T7 promoter sequence 5'-TAATACGACTCACTATAGGG-3' from cDNA. A digoxygenin (DIG)-labelled antisense RNA probe was synthesized using the DIG labelling kit (Roche) and T7 RNA polymerase according to the manufacturer's recommendations. The probe was detected with anti-DIG-AP antibody (1:2,000, Roche) and nitro-blue tetrazolium chloride (NBT)/5-bromo-4-chloro-3′-indolyphosphate (BCIP) substrate (Roche) according to published protocols. To detect the differences in expression between the mutant backgrounds and WTs after $A\beta^{short}$ and $A\beta^{long}$ injection, larvae were incubated and washed in the same tubes throughout the ISH procedure to avoid staining artefacts. To do this, larvae from different genotypes were marked by cutting the tail to allow identification after ISH. The brains were exposed by dissection, keeping the brain and spinal cord intact. Embryos were stored in 60% glycerol/PBS for imaging.

Baseline c-fos ISH:

Zebrafish larval siblings were kept in 14:10 day/night normal or reverse-cycle incubators. 50 larvae were collected at each time point (ZT1, ZT13, and ZT19) and fixed in 4% paraformaldehyde in PBS overnight. RNA in situ hybridization (ISH) to detect *c-fos* was performed as described (Thisse and Thisse, 2008).

KASP genotyping

For rapid genotyping of mutant zebrafish harbouring the *adrb2aΔ8* and *pgrmc1Δ16* alleles, a mutant allele-specific forward primer, a wild-type allele-specific forward primer and a common reverse primer were used (LGC Genomics). The primer sequences were targeted against the following;

adrb2a

5’TTTTACTACTTACTGTTTGCACAAACCTATGTTAACTGTGTTAACGTGTTTTCTTCT GCTTTTCTTTCTTGATCTCTGTCAGGTCATGGGAAACATAAGGTCCTCAATACC**[CGA AGATC/-]**TTATCTGTCCAAACAATACTAATGCCTCCACCAAAAGCGAACTACAGATG ACAGTGCTGGGCACACTCATGTCCATTCTTGTCTTGATCATCGTCTTTGGCAATGTGA TGGTGATTACAGCCA-3’

pgrmc1:

5’ATGGCTGAAGAAGCAGTCGAGCAAACTTCTGGAATCCTTCAGGAAATTTTCACGT CGCCACTGAACATCAGTTTGCTATGTCTTTGTTTGTTCCTACTTTACAAAATCATCCG CGGAGACAAGCC**[TGCAGACTATGGCCCG/-]**GYTGAGGAGCCGCTGCCCAAACT

CAAGAAAAGAGATTTYACTTTAGCAGATCTGCAAGAGTACGATGGACTGAAAAACC
CAAGAATCCTGATGGCTGTCAACGGG-3'

where [x/-] indicates the indel difference in [WT/mutant]. PCR amplification was performed using KASP Master mix (LGC Genomics) according to the manufacturer's instructions. Fluorescence was read on a CFX96 Touch Real-Time PCR Detection System (Bio-Rad) and the allelic discrimination plot generated using Bio-Rad CFX Manager Software.

Time lapse confocal microscopy

Three Casper larvae at 5 dpf were mounted dorsally on a slide in 1.5% agarose. 10 nl of Aβ42-Hi488 was intra-cardiac injected to embryos, control fish were untreated. Fish were imaged for 6 min taking 2 µm thick stacks through the whole brain using a confocal microscope (Leica SP8). Each fish was imaged every 20 mins for 8 hours.

pERK/tERK staining and activity Mapping

Larvae were fixed overnight at 4°C in 4% paraformaldehyde (PFA) and 4% sucrose in PBS; permeabilized 45 min in 0.05% trypsin-EDTA on ice; blocked 6 hr at room temperature (RT) in phosphate buffered saline plus 0.05% Triton (PBT) plus 2% normal goat serum, 1% BSA, and 1% DMSO; and then incubated over sequential nights at 4°C in primary antibodies (Cell Signaling Technology 4370 and 4696; 1:500) and secondary antibodies conjugated with Alexa fluorophores (Life Technologies; 1:200) in PBT plus 1% BSA and 1% DMSO.

Larvae were mounted in 1.5% low melt agarose and imaged with a custom two-photon microscope (Bruker; Prairie View software) with a 203 water immersion objective (Olympus). Images were noise filtered using a custom MATLAB (The MathWorks) scripts and registered into Z-Brain using the Computational Morphometry Toolkit (http://www.nitrc.org/projects/cmtk/) with the command string: -a -w -r 0102 -l af -X 52 -C 8 -G 80 -R 3 -A "–accuracy 0.4 –auto-multi-levels 4" -W "–accuracy 1.6" -T 4. Registered images were prepared using a custom MATLAB/MIJ (http://bigwww.epfl.ch/sage/soft/mij/) script to downsize, blur, and adjust the maximum brightness of each stack to the top 0.1% of pixel intensities to preserve dynamic range. Activity maps were generated using MATLAB scripts(Randlett et al., 2015).

Crispr/Cas9 mutant generation

The CRISPR design tool CHOPCHOP (http://chopchop.cbu.uib.no) was used to identify a target region in zebrafish *adrb2a* and *pgrmc1* (Labun et al., 2019). The gene specific oligomers were ordered from Thermofisher including the 5’ and 3’ tags:

For *adrb2a*:

5’ATTTAGGTGACACTATAGTTTGGACAGATAAGATCTTGTTTTAGAGCTAGAAATAG CAAG-3’

For *pgrmc1*:

5’ATTTAGGTGACACTATATGCAGACTATGGCCCGGTTGGTTTTAGAGCTAGAAATAG CAAG-3’

Constant oligomer:

5'AAAAGCACCGACTCGGTGCCACTTTTTCAAGTTGATAACGGACTAGCCTTATTTTA ACTTGCTATTTCT AGCTCTAAAAC-3'

The constant oligomer and the gene specific oligomer were annealed on a PCR machine and filled in using T4 DNA polymerase (NEB) (Gagnon et al., 2014). The template was cleaned up using a PCR clean-up column (Qiaquick) and the product was verified on a 2% agarose gel. The sgRNA was transcribed from this DNA template using Ambion MEGAscript SP6 kit (Gagnon et al., 2014). Cas9 mRNA and the purified sgRNA were co-injected into one-cell stage embryos at a concentration of 200 ng and 100 ng per embryo, respectively.

Caspase-3 staining

5dpf larvae that were injected with Aβ oligomers or soaked in Camptothecin (1µM; Sigma Aldrich) were fixed 5 hours after injection/drug treatment in 4% PFA and kept overnight at 4℃. Brains were dissected and dehydrated next day and were washed 3 times in PDT buffer (0.3 Triton-X in PBST with 1% DMSO) and incubated with Caspase-3 antibody (1:500; BD Biosciences) at 4℃. The brains were incubated with Alexa Fluor 568 goat anti-rabbit antibody (1:200; Invitrogen) next day at 4℃ overnight and imaged using a confocal microscope.

Statistical Analyses

For data analyses we used a Gardner-Altman estimation plot, which visualizes the effect size and displays an experimental dataset's complete statistical information (Ho et al., 2019). The bootstrapped 95% confidence interval (CI) was calculated from 10,000 bootstrapped resamples (Ho et al., 2019).

Details of statistics used in each panel are also described in the figure legend. For multiple comparisons, data was first tested for normality by the Kogloromov-Smirnov (KS) statistic and extreme outliers were discarded by Grubb's test ($p \leq 0.01$). Those that violated normality were analysed with the non-parametric Kruskal-Wallis test, with either Tukey-Kramer or Bonferonni post hoc testing; otherwise, data was analysed with one-way ANOVA followed by Tukey's post-hoc testing. For dose response curves, a two-way ANOVA was performed to test the interaction effects between preparation type and dose. For return to baseline statistics, paired t-tests were performed. Survival curves were analysed with Kaplan-Meier log rank test. All statistical tests and graphs were generated in MATLAB (R2015a) loaded with the Statistical Toolbox. Injection and tracking experiments were performed blinded.

REFERENCES:

Allen, S.R., Seiler, W.O., Stahelin, H.B., and Spiegel, R. (1987). Seventy-two hour polygraphic and behavioral recordings of wakefulness and sleep in a hospital geriatric unit: comparison between demented and nondemented patients. Sleep *10*, 143-159.

Amrhein, V., Greenland, S., and McShane, B. (2019). Scientists rise up against statistical significance. Nature *567*, 305-307.

Ashlin, T.G., Blunsom, N.J., Ghosh, M., Cockcroft, S., and Rihel, J. (2018). Pitpnc1a Regulates Zebrafish Sleep and Wake Behavior through Modulation of Insulin-like Growth Factor Signaling. Cell Rep *24*, 1389-1396.

Baraban, S.C., Taylor, M.R., Castro, P.A., and Baier, H. (2005). Pentylenetetrazole induced changes in zebrafish behavior, neural activity and c-fos expression. Neuroscience *131*, 759-768.

781 Barlow, I.L., and Rihel, J. (2017). Zebrafish sleep: from geneZZZ to neuronZZZ. Curr Opin
782 Neurobiol *44*, 65-71.

783 Bateman, R.J., Wen, G., Morris, J.C., and Holtzman, D.M. (2007). Fluctuations of CSF amyloid-
784 beta levels: implications for a diagnostic and therapeutic biomarker. Neurology *68*, 666-669.

785 Benilova, I., Karran, E., and De Strooper, B. (2012). The toxic Abeta oligomer and Alzheimer's
786 disease: an emperor in need of clothes. Nat Neurosci *15*, 349-357.

787 Cirrito, J.R., Yamada, K.A., Finn, M.B., Sloviter, R.S., Bales, K.R., May, P.C., Schoepp, D.D.,
788 Paul, S.M., Mennerick, S., and Holtzman, D.M. (2005). Synaptic activity regulates interstitial
789 fluid amyloid-beta levels in vivo. Neuron *48*, 913-922.

790 Cotto, E., Andre, M., Forgue, J., Fleury, H.J., and Babin, P.J. (2005). Molecular characterization,
791 phylogenetic relationships, and developmental expression patterns of prion genes in zebrafish
792 (Danio rerio). Febs j *272*, 500-513.

793 De, S., Wirthensohn, D.C., Flagmeier, P., Hughes, C., Aprile, F.A., Ruggeri, F.S., Whiten, D.R.,
794 Emin, D., Xia, Z., Varela, J.A., *et al.* (2019). Different soluble aggregates of Abeta42 can give
795 rise to cellular toxicity through different mechanisms. Nat Commun *10*, 1541.

796 Eimer, W.A., Vijaya Kumar, D.K., Navalpur Shanmugam, N.K., Rodriguez, A.S., Mitchell, T.,
797 Washicosky, K.J., Gyorgy, B., Breakefield, X.O., Tanzi, R.E., and Moir, R.D. (2018).
798 Alzheimer's Disease-Associated beta-Amyloid Is Rapidly Seeded by Herpesviridae to Protect
799 against Brain Infection. Neuron *100*, 1527-1532.

800 Fleisch, V.C., Leighton, P.L., Wang, H., Pillay, L.M., Ritzel, R.G., Bhinder, G., Roy, B.,
801 Tierney, K.B., Ali, D.W., Waskiewicz, A.J., *et al.* (2013). Targeted mutation of the gene
802 encoding prion protein in zebrafish reveals a conserved role in neuron excitability. Neurobiol Dis
803 *55*, 11-25.

804 Fronczek, R., van Geest, S., Frolich, M., Overeem, S., Roelandse, F.W., Lammers, G.J., and
805 Swaab, D.F. (2012). Hypocretin (orexin) loss in Alzheimer's disease. Neurobiol Aging *33*, 1642-
806 1650.

807 Gagnon, J.A., Valen, E., Thyme, S.B., Huang, P., Akhmetova, L., Pauli, A., Montague, T.G.,
808 Zimmerman, S., Richter, C., and Schier, A.F. (2014). Efficient mutagenesis by Cas9 protein-
809 mediated oligonucleotide insertion and large-scale assessment of single-guide RNAs. PLoS One
810 *9*, e98186.

811 Ghavami, M., Rezaei, M., Ejtehadi, R., Lotfi, M., Shokrgozar, M.A., Abd Emamy, B., Raush, J.,
812 and Mahmoudi, M. (2013). Physiological temperature has a crucial role in amyloid beta in the
813 absence and presence of hydrophobic and hydrophilic nanoparticles. ACS Chem Neurosci *4*,
814 375-378.

815 Gimbel, D.A., Nygaard, H.B., Coffey, E.E., Gunther, E.C., Lauren, J., Gimbel, Z.A., and
816 Strittmatter, S.M. (2010). Memory impairment in transgenic Alzheimer mice requires cellular
817 prion protein. J Neurosci *30*, 6367-6374.

818 Ho, J., Tumkaya, T., Aryal, S., Choi, H., and Claridge-Chang, A. (2019). Moving beyond P
819 values: data analysis with estimation graphics. Nat Methods *16*, 565-566.

820 Imeri, L., and Opp, M.R. (2009). How (and why) the immune system makes us sleep. Nat Rev
821 Neurosci *10*, 199-210.

822 Irizarry, M.C., McNamara, M., Fedorchak, K., Hsiao, K., and Hyman, B.T. (1997). APPSw
823 transgenic mice develop age-related A beta deposits and neuropil abnormalities, but no neuronal
824 loss in CA1. J Neuropathol Exp Neurol *56*, 965-973.

825 Izzo, N.J., Staniszewski, A., To, L., Fa, M., Teich, A.F., Saeed, F., Wostein, H., Walko, T., 3rd,
826 Vaswani, A., Wardius, M., *et al.* (2014a). Alzheimer's therapeutics targeting amyloid beta 1-42
827 oligomers I: Abeta 42 oligomer binding to specific neuronal receptors is displaced by drug
828 candidates that improve cognitive deficits. PLoS One *9*, e111898.

829 Izzo, N.J., Xu, J., Zeng, C., Kirk, M.J., Mozzoni, K., Silky, C., Rehak, C., Yurko, R., Look, G.,
830 Rishton, G., *et al.* (2014b). Alzheimer's therapeutics targeting amyloid beta 1-42 oligomers II:
831 Sigma-2/PGRMC1 receptors mediate Abeta 42 oligomer binding and synaptotoxicity. PLoS One
832 *9*, e111899.

833 Jack, C.R., Jr., Knopman, D.S., Jagust, W.J., Petersen, R.C., Weiner, M.W., Aisen, P.S., Shaw,
834 L.M., Vemuri, P., Wiste, H.J., Weigand, S.D., *et al.* (2013). Tracking pathophysiological
835 processes in Alzheimer's disease: an updated hypothetical model of dynamic biomarkers. Lancet
836 Neurol *12*, 207-216.

837 Jarosz-Griffiths, H.H., Noble, E., Rushworth, J.V., and Hooper, N.M. (2016). Amyloid-beta
838 Receptors: The Good, the Bad, and the Prion Protein. J Biol Chem *291*, 3174-3183.

839 Kamenetz, F., Tomita, T., Hsieh, H., Seabrook, G., Borchelt, D., Iwatsubo, T., Sisodia, S., and
840 Malinow, R. (2003). APP processing and synaptic function. Neuron *37*, 925-937.

841 Kang, J.E., Lim, M.M., Bateman, R.J., Lee, J.J., Smyth, L.P., Cirrito, J.R., Fujiki, N., Nishino,
842 S., and Holtzman, D.M. (2009). Amyloid-beta dynamics are regulated by orexin and the sleep-
843 wake cycle. Science *326*, 1005-1007.

844 Kokel, D., Bryan, J., Laggner, C., White, R., Cheung, C.Y., Mateus, R., Healey, D., Kim, S.,
845 Werdich, A.A., Haggarty, S.J., *et al.* (2010). Rapid behavior-based identification of neuroactive
846 small molecules in the zebrafish. Nat Chem Biol *6*, 231-237.

847 Kostylev, M.A., Kaufman, A.C., Nygaard, H.B., Patel, P., Haas, L.T., Gunther, E.C., Vortmeyer,
848 A., and Strittmatter, S.M. (2015). Prion-Protein-interacting Amyloid-beta Oligomers of High
849 Molecular Weight Are Tightly Correlated with Memory Impairment in Multiple Alzheimer
850 Mouse Models. J Biol Chem *290*, 17415-17438.

851 Kumar, D.K., Choi, S.H., Washicosky, K.J., Eimer, W.A., Tucker, S., Ghofrani, J., Lefkowitz,
852 A., McColl, G., Goldstein, L.E., Tanzi, R.E., *et al.* (2016). Amyloid-beta peptide protects against
853 microbial infection in mouse and worm models of Alzheimer's disease. Sci Transl Med *8*,
854 340ra372.

855 Kusumoto, Y., Lomakin, A., Teplow, D.B., and Benedek, G.B. (1998). Temperature dependence
856 of amyloid beta-protein fibrillization. Proc Natl Acad Sci U S A *95*, 12277-12282.

857 Labun, K., Montague, T.G., Krause, M., Torres Cleuren, Y.N., Tjeldnes, H., and Valen, E.
858 (2019). CHOPCHOP v3: expanding the CRISPR web toolbox beyond genome editing. Nucleic
859 Acids Res *47*, W171-w174.

860 Lauren, J., Gimbel, D.A., Nygaard, H.B., Gilbert, J.W., and Strittmatter, S.M. (2009). Cellular
861 prion protein mediates impairment of synaptic plasticity by amyloid-beta oligomers. Nature *457*,
862 1128-1132.

863 Leighton, P.L.A., Kanyo, R., Neil, G.J., Pollock, N.M., and Allison, W.T. (2018). Prion gene
864 paralogs are dispensable for early zebrafish development and have nonadditive roles in seizure
865 susceptibility. J Biol Chem *293*, 12576-12592.

866 Lesne, S.E., Sherman, M.A., Grant, M., Kuskowski, M., Schneider, J.A., Bennett, D.A., and
867 Ashe, K.H. (2013). Brain amyloid-beta oligomers in ageing and Alzheimer's disease. Brain *136*,
868 1383-1398.

869 Lim, A.S., Ellison, B.A., Wang, J.L., Yu, L., Schneider, J.A., Buchman, A.S., Bennett, D.A., and
870 Saper, C.B. (2014). Sleep is related to neuron numbers in the ventrolateral preoptic/intermediate
871 nucleus in older adults with and without Alzheimer's disease. Brain *137*, 2847-2861.

872 Loewenstein, R.J., Weingartner, H., Gillin, J.C., Kaye, W., Ebert, M., and Mendelson, W.B.
873 (1982). Disturbances of sleep and cognitive functioning in patients with dementia. Neurobiol
874 Aging *3*, 371-377.

875 Malaga-Trillo, E., Solis, G.P., Schrock, Y., Geiss, C., Luncz, L., Thomanetz, V., and Stuermer,
876 C.A. (2009). Regulation of embryonic cell adhesion by the prion protein. PLoS Biol *7*, e55.

877 Manaye, K.F., Mouton, P.R., Xu, G., Drew, A., Lei, D.L., Sharma, Y., Rebeck, G.W., and
878 Turner, S. (2013). Age-related loss of noradrenergic neurons in the brains of triple transgenic
879 mice. Age (Dordr) *35*, 139-147.

880 Moir, R.D., and Tanzi, R.E. (2019). Low Evolutionary Selection Pressure in Senescence Does
881 Not Explain the Persistence of Abeta in the Vertebrate Genome. Front Aging Neurosci *11*, 70.

882 Moran, M., Lynch, C.A., Walsh, C., Coen, R., Coakley, D., and Lawlor, B.A. (2005). Sleep
883 disturbance in mild to moderate Alzheimer's disease. Sleep Med *6*, 347-352.

884 Newman, M., Ebrahimie, E., and Lardelli, M. (2014). Using the zebrafish model for Alzheimer's
885 disease research. Front Genet *5*, 189.

886 Nicoll, A.J., Panico, S., Freir, D.B., Wright, D., Terry, C., Risse, E., Herron, C.E., O'Malley, T.,
887 Wadsworth, J.D., Farrow, M.A., *et al.* (2013). Amyloid-beta nanotubes are associated with prion
888 protein-dependent synaptotoxicity. Nat Commun *4*, 2416.

889 Nygaard, H.B., van Dyck, C.H., and Strittmatter, S.M. (2014). Fyn kinase inhibition as a novel
890 therapy for Alzheimer's disease. Alzheimers Res Ther *6*, 8.

891 O'Brien, R.J., and Wong, P.C. (2011). Amyloid precursor protein processing and Alzheimer's
892 disease. Annu Rev Neurosci *34*, 185-204.

893 Orban, G., Volgyi, K., Juhasz, G., Penke, B., Kekesi, K.A., Kardos, J., and Czurko, A. (2010).
894 Different electrophysiological actions of 24- and 72-hour aggregated amyloid-beta oligomers on
895 hippocampal field population spike in both anesthetized and awake rats. Brain Res *1354*, 227-
896 235.

897 Prinz, P.N., Vitaliano, P.P., Vitiello, M.V., Bokan, J., Raskind, M., Peskind, E., and Gerber, C.
898 (1982). Sleep, EEG and mental function changes in senile dementia of the Alzheimer's type.
899 Neurobiol Aging *3*, 361-370.

900 Prober, D.A., Rihel, J., Onah, A.A., Sung, R.J., and Schier, A.F. (2006). Hypocretin/orexin
901 overexpression induces an insomnia-like phenotype in zebrafish. J Neurosci *26*, 13400-13410.

902 Randlett, O., Wee, C.L., Naumann, E.A., Nnaemeka, O., Schoppik, D., Fitzgerald, J.E.,
903 Portugues, R., Lacoste, A.M., Riegler, C., Engert, F., *et al.* (2015). Whole-brain activity mapping
904 onto a zebrafish brain atlas. Nat Methods *12*, 1039-1046.

905 Rihel, J., Prober, D.A., Arvanites, A., Lam, K., Zimmerman, S., Jang, S., Haggarty, S.J., Kokel,
906 D., Rubin, L.L., Peterson, R.T., *et al.* (2010). Zebrafish behavioral profiling links drugs to
907 biological targets and rest/wake regulation. Science *327*, 348-351.

908 Risse, E., Nicoll, A.J., Taylor, W.A., Wright, D., Badoni, M., Yang, X., Farrow, M.A., and
909 Collinge, J. (2015). Identification of a Compound That Disrupts Binding of Amyloid-beta to the
910 Prion Protein Using a Novel Fluorescence-based Assay. J Biol Chem *290*, 17020-17028.

911 Roh, J.H., Huang, Y., Bero, A.W., Kasten, T., Stewart, F.R., Bateman, R.J., and Holtzman, D.M.
912 (2012). Disruption of the sleep-wake cycle and diurnal fluctuation of beta-amyloid in mice with
913 Alzheimer's disease pathology. Sci Transl Med *4*, 150ra122.

914 Roy, S.J., Glazkova, I., Frechette, L., Iorio-Morin, C., Binda, C., Petrin, D., Trieu, P., Robitaille,
915 M., Angers, S., Hebert, T.E., *et al.* (2013). Novel, gel-free proteomics approach identifies RNF5
916 and JAMP as modulators of GPCR stability. Mol Endocrinol *27*, 1245-1266.

917 Shokri-Kojori, E., Wang, G.J., Wiers, C.E., Demiral, S.B., Guo, M., Kim, S.W., Lindgren, E.,
918 Ramirez, V., Zehra, A., Freeman, C., *et al.* (2018). beta-Amyloid accumulation in the human
919 brain after one night of sleep deprivation. Proc Natl Acad Sci U S A *115*, 4483-4488.

920 Soscia, S.J., Kirby, J.E., Washicosky, K.J., Tucker, S.M., Ingelsson, M., Hyman, B., Burton,
921 M.A., Goldstein, L.E., Duong, S., Tanzi, R.E., *et al.* (2010). The Alzheimer's disease-associated
922 amyloid beta-protein is an antimicrobial peptide. PLoS One *5*, e9505.

923 Steele, S.L., Yang, X., Debiais-Thibaud, M., Schwerte, T., Pelster, B., Ekker, M., Tiberi, M., and
924 Perry, S.F. (2011). In vivo and in vitro assessment of cardiac beta-adrenergic receptors in larval
925 zebrafish (Danio rerio). J Exp Biol *214*, 1445-1457.

926 Sterniczuk, R., Antle, M.C., Laferla, F.M., and Dyck, R.H. (2010). Characterization of the 3xTg-
927 AD mouse model of Alzheimer's disease: part 2. Behavioral and cognitive changes. Brain Res
928 *1348*, 149-155.

929 Szaruga, M., Munteanu, B., Lismont, S., Veugelen, S., Horre, K., Mercken, M., Saido, T.C.,
930 Ryan, N.S., De Vos, T., Savvides, S.N., *et al.* (2017). Alzheimer's-Causing Mutations Shift
931 Abeta Length by Destabilizing gamma-Secretase-Abetan Interactions. Cell *170*, 443-456.e414.

932 Thisse, B., Thisse, C. (2004). Fast Release Clones: A High Throughput Expression Analysis.
933 ZFIN Direct Data Submission (http://zfin.org).

934 Thisse, C., and Thisse, B. (2008). High-resolution in situ hybridization to whole-mount zebrafish
935 embryos. Nat Protoc *3*, 59-69.

936 Um, J.W., Kaufman, A.C., Kostylev, M., Heiss, J.K., Stagi, M., Takahashi, H., Kerrisk, M.E.,
937 Vortmeyer, A., Wisniewski, T., Koleske, A.J., *et al.* (2013). Metabotropic glutamate receptor 5 is
938 a coreceptor for Alzheimer abeta oligomer bound to cellular prion protein. Neuron *79*, 887-902.

939 Um, J.W., Nygaard, H.B., Heiss, J.K., Kostylev, M.A., Stagi, M., Vortmeyer, A., Wisniewski,
940 T., Gunther, E.C., and Strittmatter, S.M. (2012). Alzheimer amyloid-beta oligomer bound to
941 postsynaptic prion protein activates Fyn to impair neurons. Nat Neurosci *15*, 1227-1235.

942 Vazquez de la Torre, A., Gay, M., Vilaprinyo-Pascual, S., Mazzucato, R., Serra-Batiste, M.,
943 Vilaseca, M., and Carulla, N. (2018). Direct Evidence of the Presence of Cross-Linked Abeta
944 Dimers in the Brains of Alzheimer's Disease Patients. Anal Chem *90*, 4552-4560.

945 Videnovic, A., Lazar, A.S., Barker, R.A., and Overeem, S. (2014). 'The clocks that time us'--
946 circadian rhythms in neurodegenerative disorders. Nat Rev Neurol *10*, 683-693.

947 Wang, D., Govindaiah, G., Liu, R., De Arcangelis, V., Cox, C.L., and Xiang, Y.K. (2010).
948 Binding of amyloid beta peptide to beta2 adrenergic receptor induces PKA-dependent AMPA
949 receptor hyperactivity. Faseb j *24*, 3511-3521.

950 Wang, J., Ikonen, S., Gurevicius, K., van Groen, T., and Tanila, H. (2002). Alteration of cortical
951 EEG in mice carrying mutated human APP transgene. Brain Res *943*, 181-190.

952 Wang, Z., Nishimura, Y., Shimada, Y., Umemoto, N., Hirano, M., Zang, L., Oka, T., Sakamoto,
953 C., Kuroyanagi, J., and Tanaka, T. (2009). Zebrafish beta-adrenergic receptor mRNA expression
954 and control of pigmentation. Gene *446*, 18-27.

955 Whitcomb, D.J., Hogg, E.L., Regan, P., Piers, T., Narayan, P., Whitehead, G., Winters, B.L.,
956 Kim, D.H., Kim, E., St George-Hyslop, P., *et al.* (2015). Intracellular oligomeric amyloid-beta
957 rapidly regulates GluA1 subunit of AMPA receptor in the hippocampus. Sci Rep *5*, 10934.

958 Xie, L., Kang, H., Xu, Q., Chen, M.J., Liao, Y., Thiyagarajan, M., O'Donnell, J., Christensen,
959 D.J., Nicholson, C., Iliff, J.J., *et al.* (2013). Sleep drives metabolite clearance from the adult
960 brain. Science *342*, 373-377.

961

962

Supplemental Information

Figure 1 – figure supplement 1. Aβ oligomers exert dose-dependent, short-term effects on zebrafish sleep

A) Same images from Figure 1B, highlighting the region of interest in the telencephalon for fluorescence intensity measurements in B. Anterior is to the top, dorsal view.

B) Heart-injected fluorescently-tagged Aβ (black) penetrates the brain within 1 hr and peaks in concentration 2-3 hr post-injection. Cyan shows background fluorescence of a negative control. The shaded area shows ± standard deviation from 3 independent injections.

C) Electron micrographs of Aβ oligomers formed after 24 hr incubation at 4°C, 25°C, and 37°C. $A\beta^{arctic}$ was incubated at 25°C for 2 hr as a positive control. The color code is used throughout the main and supplementary figures. Scale bar = 100 nm

D) The $A\beta^{short}$ (blue) and $A\beta^{long}$ (green) have opposing, dose-dependent effects on average waking activity, normalized to $A\beta^{rev}$ injections. The error bars represent ± the SEM. doseXprep interaction *p≤0.05, ****p≤0.0001 two-way ANOVA, Fisher's least significant difference post hoc test. p≤0.001, prep effect (plotted in F).

E) $A\beta^{short}$ (blue) and $A\beta^{long}$ (green) have opposing, dose-dependent effects on sleep. doseXprep interaction, two-way ANOVA, *p≤0.05, Fisher's least significant difference post hoc test. p≤0.05, prep effect (plotted in G). Based on the data in D-E, 10nM was chosen as the concentration for all subsequent Aβ injection experiments.

F) The waking activity for each larva in D, normalized to $A\beta^{rev}$ injections and plotted to emphasize the significant effect of the preparation irrespective of dose (p<0.001, two-way ANOVA).

G) Sleep for each larva in E normalized to $A\beta^{rev}$ injections and plotted to emphasize the significant effect of the preparation ($p<0.001$, two-way ANOVA).

H) Sleep plot of untreated WT (black), anesthetized only (red), mock injected (blue) and PBS injected (green) fish on a 14hr:10hr light:dark cycle (indicated by the white and black bars). The ribbons represent ± the SEM.

I) Sleep for each larva in H (WT (black), anesthetised only (red), mock injected (blue) and PBS injected (green)) shows that there is no statistical difference in sleep due to any of the manipulations ($p>0.05$, one-way ANOVA).

J) Sleep plot after vehicle injection (PBS, magenta trace) and immediate tracking compared to larvae that had acclimated to the apparatus for 24 hrs (black trace). The ribbons represent ± the SEM. Gold stars flag significantly different timepoints ($p<0.05$, repeated measures ANOVA) and were used to determine the window for calculating the evening-only effects of Aβ injections.

K) Calculating Aβ injection effects across the whole day or only in the evening window (data from Figure 1) has minimal effect on the analysis of $A\beta^{short}$ or $A\beta^{long}$. The only exception (red shading) is for the reduction in sleep by $A\beta^{short}$, due to a flooring effect.

Figure 1- figure supplement 2. Aβ exposure does not increase neuronal cell death and does not alter survival into adulthood.

A) Dorsal and ventral views of representative 5 dpf larval brains stained for Caspase-3 activation (purple) to map apoptosis. Exposure to the topoisomerase inhibitor camptothecin (CPT, 1µM), which induces apoptosis, serves as a positive control. DAPI stains nuclei in white for reference. Anterior is to the left. Scale bar = 100 µm

B,C) Quantification of the number of Caspase-3 positive cells after exposure to 1µM CPT or Aβ oligomer injections (n=5 brains for each condition, B-dorsal, C-ventral). Only CPT significantly increased apoptosis relative to $A\beta^{rev}$. ns, $p>0.05$, one-way ANOVA, Tukey's post-hoc test.

D) Survival curves to adulthood after 5dpf injection of Aβ oligomers. There are no significant differences among survival curves, $p>0.05$, Kaplan-Meier log rank test.

Figure 1- figure supplement 3. Aβ-injected larvae recover after 24 hrs and do not exhibit seizure-like or sickness behavior.

A-B) The effects of $A\beta^{short}$ (A) and $A\beta^{long}$ (B) on waking activity (top) and sleep (bottom) return to baseline after 24hr. Shown in A and B are traces for 48 hours post-injection on a 14hr:10hr light:dark cycle (indicated by the white and black bars). The ribbons represent ± the SEM. Plotted on the right are the percent change induced by Aβ relative to $A\beta^{rev}$ for day 1 versus day 2, demonstrating that these parameters return to baseline (*$p\leq0.01$, paired t-test). Each line represents a single larva, the thicker line represents the mean ± SEM.

C) Activity traces of $A\beta^{short}$ (blue), $A\beta^{long}$ (green), and $A\beta^{rev}$ (black) during and after a ten minute dark pulse are indistinguishable. Traces are for a 10 min:10min:10 min light:dark:light window (indicated by the white and black bars). The ribbons represent ± the SEM.

D) The effects of $A\beta^{rev}$ (black), convulsant PTZ (10 mM, orange), $A\beta^{short}$ (blue), and $A\beta^{long}$ (green) on sub-second larval bout structures. Shown are delta pixel movement of one representative larva in each group for ~1 min (see Figure 1-video 1). Unlike PTZ treated larvae, Aβ injected larvae have normal bout structures. Representative larvae were chosen to also highlight that, while overall $A\beta^{long}$ injected larvae are less active, individual animals can have

sustained periods of heightened activity. Similarly, individual $A\beta^{short}$ injected animals can exhibit periods of relatively dampened activity.

E) The effects of $A\beta^{rev}$ (black), convulsant PTZ (10 mM, orange), $A\beta^{short}$ (blue) and $A\beta^{long}$ (green) on high frequency bouts (HFB) in a 5 minute interval. Each dot represents a single larva. PTZ induced HFB's is non-existent or very rare in the other groups (n=24 for all groups).

Figure 3- figure supplement 1. Crispr/Cas9 targeting of zebrafish *adrb2a* and *pgrmc1*

A) Human PGRMC1and zebrafish Pgrmc1 contain a conserved Transmembrane (TM) domain (yellow) and a Cytochrome b5-like Heme/Steroid binding domain (blue).

B) Protein alignment of zebrafish Pgrmc1 to human PGRMC1. Identical residues are marked in black, similar residues in grey.

C) Crispr-Cas9 targeting of *pgrmc1* generated an allele with a 16bp deletion. The PAM sequence is indicated in red.

D) The predicted translation of *pgrmc1* Δ16 leads to a premature stop codon.

E) Protein alignment of zebrafish Adrb2a and Adrb2b to human ADRB2. Identical residues are marked in black, similar residues in grey. The N-terminal region (pink) is the putative Aβ binding region. The C-terminal region is in green.

F) Crispr-Cas9 targeting of *adrb2a* generated an allele with an 8bp deletion. The PAM sequence is indicated in red.

G) The predicted translation of *adrb2a*Δ8 leads to a premature stop codon lacking all functional domains.

Figure 3- figure supplement 2. *adrb2a* and *pgrmc1* mutations have small effects on baseline sleep:wake parameters.

A-C') Sleep and waking activity plots for larvae from *pgrmc1*$^{+/-}$ in-crosses. A,A') show representative 48hr traces for the indicated genotypes. The ribbon represents ± SEM. B-C') Sleep and waking activity for each larva for all genotypes are plotted. The error bars represent the mean ± SEM. There is a trend to decreased waking activity in *pgrmc1*$^{-/-}$ mutants compared to wild type siblings. p=0.07, Kruskal-Wallis, Tukey-Kramer post-hoc.

D-F') Sleep and waking activity plots for larvae from *adrb2a*$^{+/-}$ in-crosses. D,D') show 48 hr traces for all three genotypes. The ribbon represents ± SEM. E-F') Sleep and waking activity for the day and night are plotted for each larva. The error bars represent the mean ± SEM. Compared to both wild type and heterozygous siblings, *adrb2a*$^{-/-}$ mutants have increased sleep during the day. *p≤0.05, Kruskal-Wallis, Tukey-Kramer post-hoc.

Figure 4- figure supplement 1. Relationship among zebrafish *prp* genes with Aβ binding sites

A) Schematic comparing zebrafish Prp1-3 proteins to human PrP. SP, signal peptide (dark grey); R, repetitive region (blue); HD, hydrophobic domain (yellow); N, glycosylation sites (black lines); GPI anchor residue (triangle); hydrophobic tail (coral). Aβ oligomer binding regions are shown in red. Breakpoints at repetitive regions indicate length variation. Adapted from (Cotto et al., 2005).

B) Protein alignments of zebrafish Prp1, Prp2, and Prp3 proteins to human and mouse PrP proteins. Identical residues are marked in black, similar residues in grey. Aβ oligomer binding

sites are indicated in red. The site of truncation mutations in *prp1* and *prp2* mutants are indicated with a triangle.

Figure 4- figure supplement 2. *prp* double mutants do not affect baseline sleep or wake across the day:night cycle.

A-C') Sleep and waking activity plots for larvae from $prp1^{+/-}; prp2^{+/-}$ in-crosses. A,A') show representative 48hr traces for the indicated genotypes. The ribbon represents ± SEM. B-C') Sleep and waking activity for each larva for all genotypes are plotted. The error bars represent the mean ± SEM.

D-F') Sleep and waking activity plots for larvae from $prp1^{+/-};prp2^{-/-}$ in-crosses. D, D') show 48 hr traces for all three genotypes. The ribbon represents ± SEM. E-F') Sleep and waking activity for the day and night are plotted for each larva. The error bars represent the mean ± SEM.

Figure 6-figure supplement 1. Pharmacological blockade of the AB^{long}-Prp-MgluR5-Fyn Kinase signalling cascade prevents reductions in waking activity

A) Representative traces of waking activity after $A\beta^{long}$ versus $A\beta^{rev}$ injections in wild type larvae in the absence (left) or presence (right) of the Aβ-Prp binding disruptor, Chicago Sky Blue (3nM). The data are from the same injections as in Figures 6B. Ribbons represent ± SEM. Light and dark bars indicate the lights ON and lights OFF periods, respectively.

B) The change in normalized waking activity induced by $A\beta^{long}$ versus $A\beta^{rev}$ control injections in the absence or presence of 3nM Chicago Sky Blue. Each dot represents a single larva and error bars indicate ± SEM. The mean difference effect size and 95% confidence interval is plotted at

the bottom. N= the number of larvae in each group. **p≤0.01, Kruskal-Wallis, Tukey-Kramer post hoc.

C) Representative traces of sleep behavior after $A\beta^{long}$ versus $A\beta^{rev}$ injections (left) in the presence of the mGluR5 inhibitor, MPEP (5 μM) and (right) Src-kinase inhibitor, saracatinib (300nM). Ribbons represent ± SEM. The data are from the same injections as in Fig. 6D.

D) The change in sleep induced by $A\beta^{long}$ relative to $A\beta^{rev}$ control injections in the presence of MPEP (5 μM) and (300nM) saracatinib. *p≤0.05, **p≤0.01, Kruskal-Wallis, Tukey-Kramer post hoc.

Figure 2- source data 1. MAP-Mapping of brain areas that are significantly up- and down-regulated in P-ERK levels in response to $A\beta^{short}$

Figure 2- source data 2. MAP-Mapping of brain areas that are significantly up- and down-regulated in P-ERK levels in response to $A\beta^{short}$

Figure 1- video 1. Aβ does not induce seizures.

Figure 1

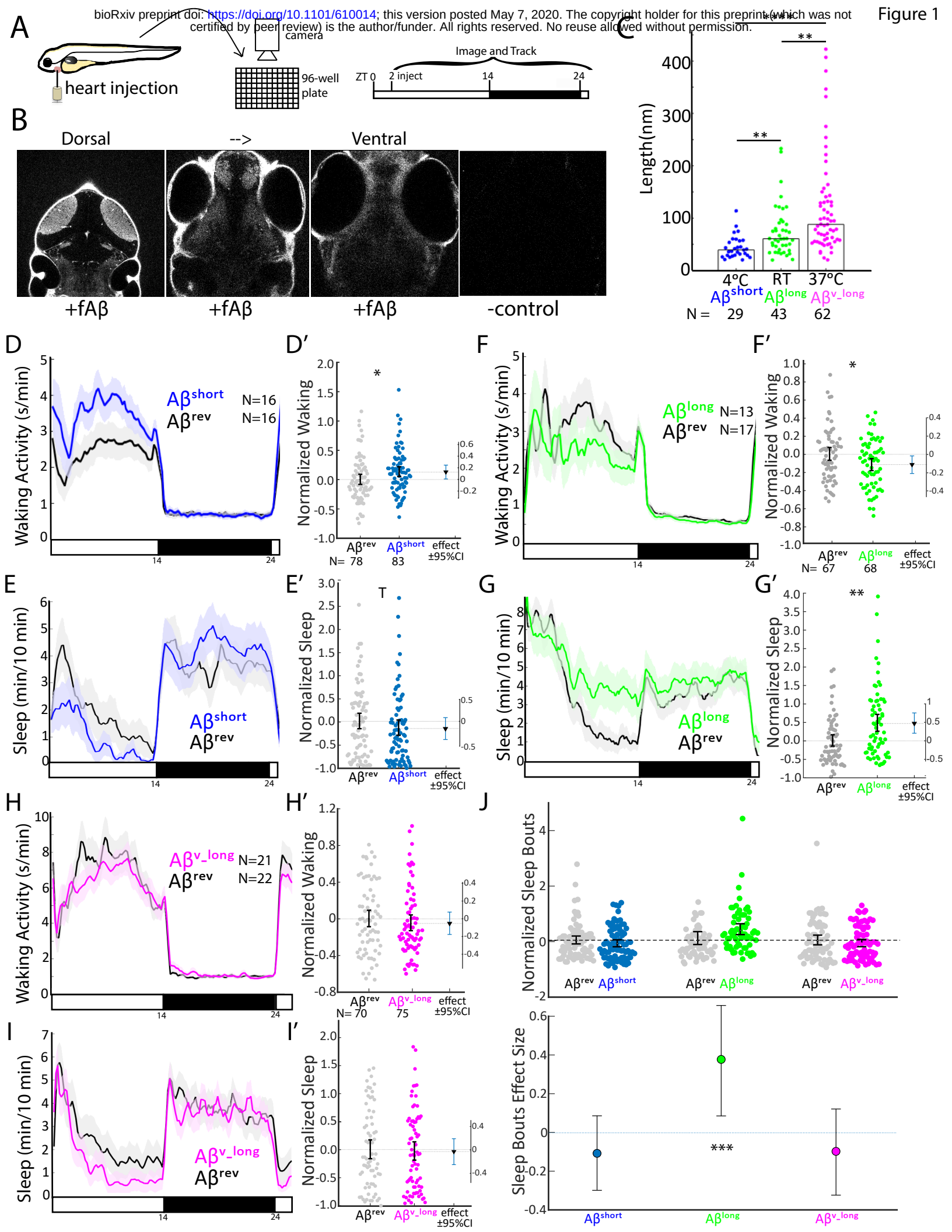

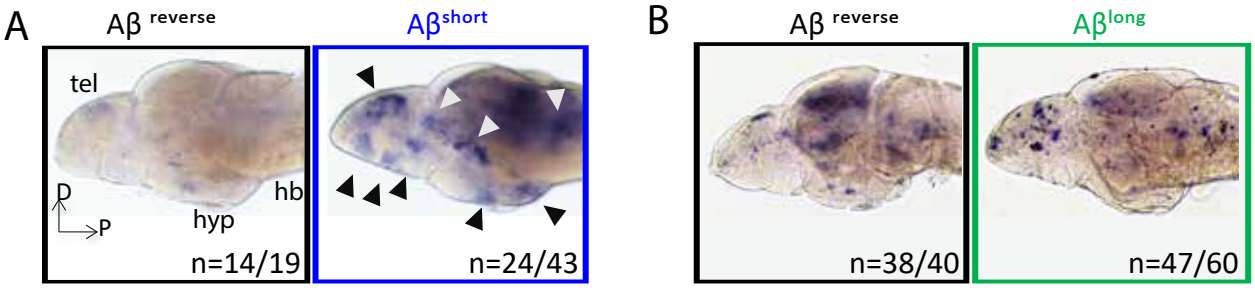

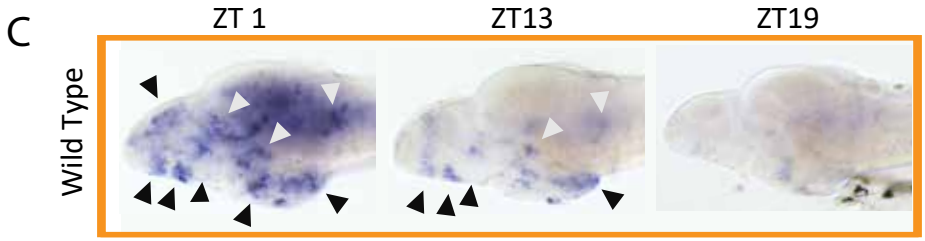

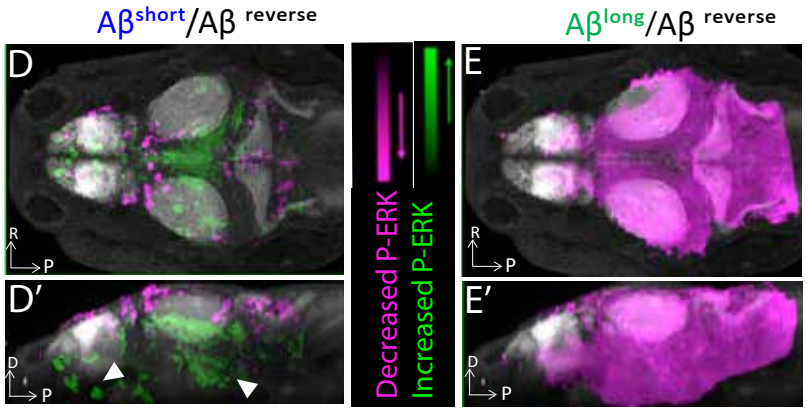

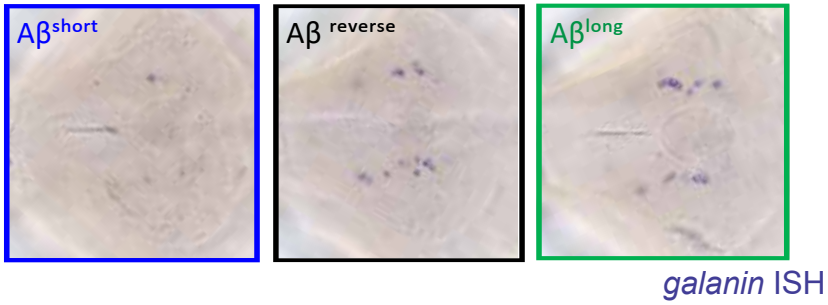

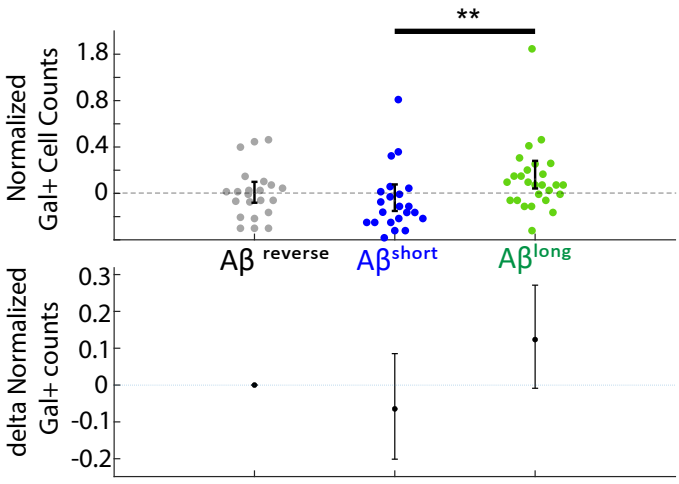

Figure 2

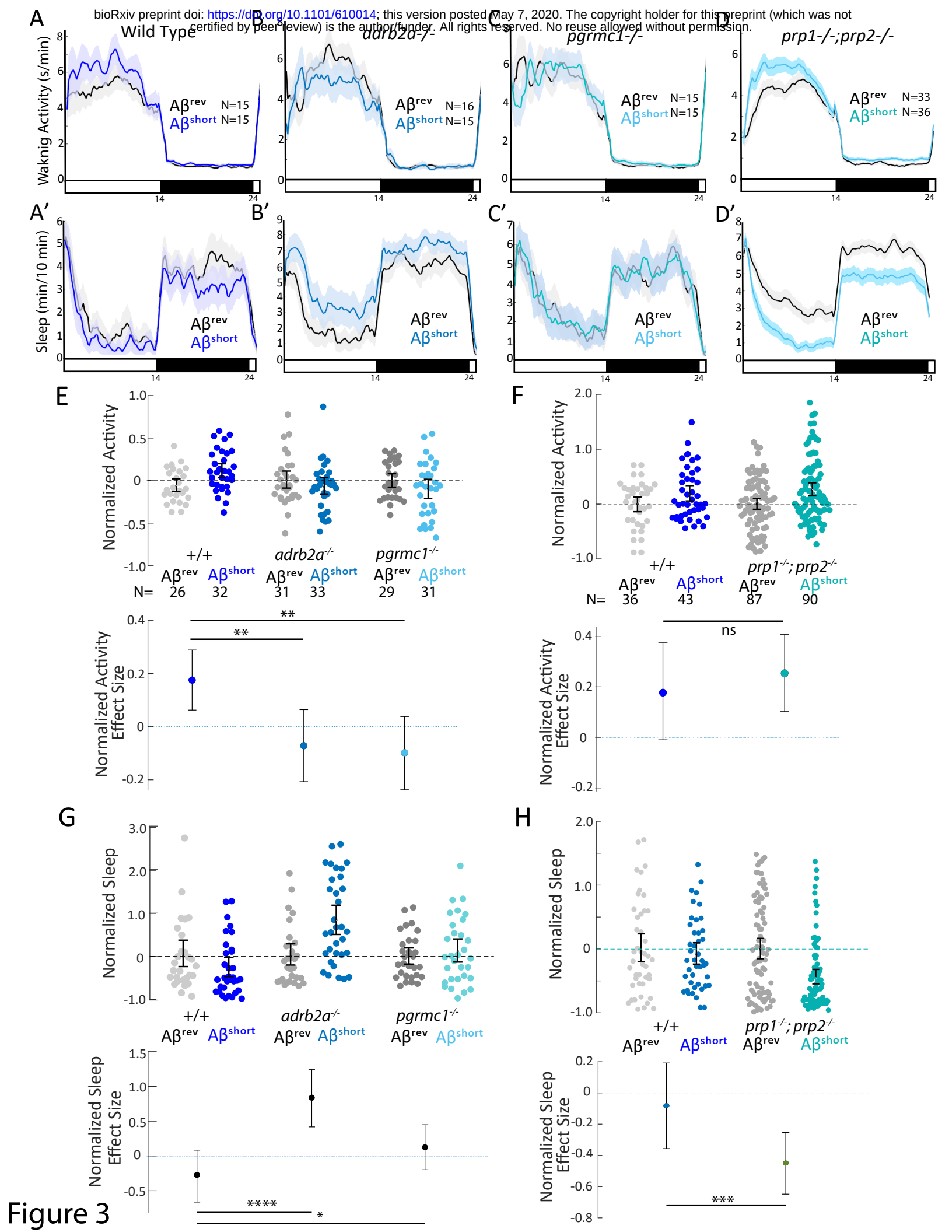

Figure 3

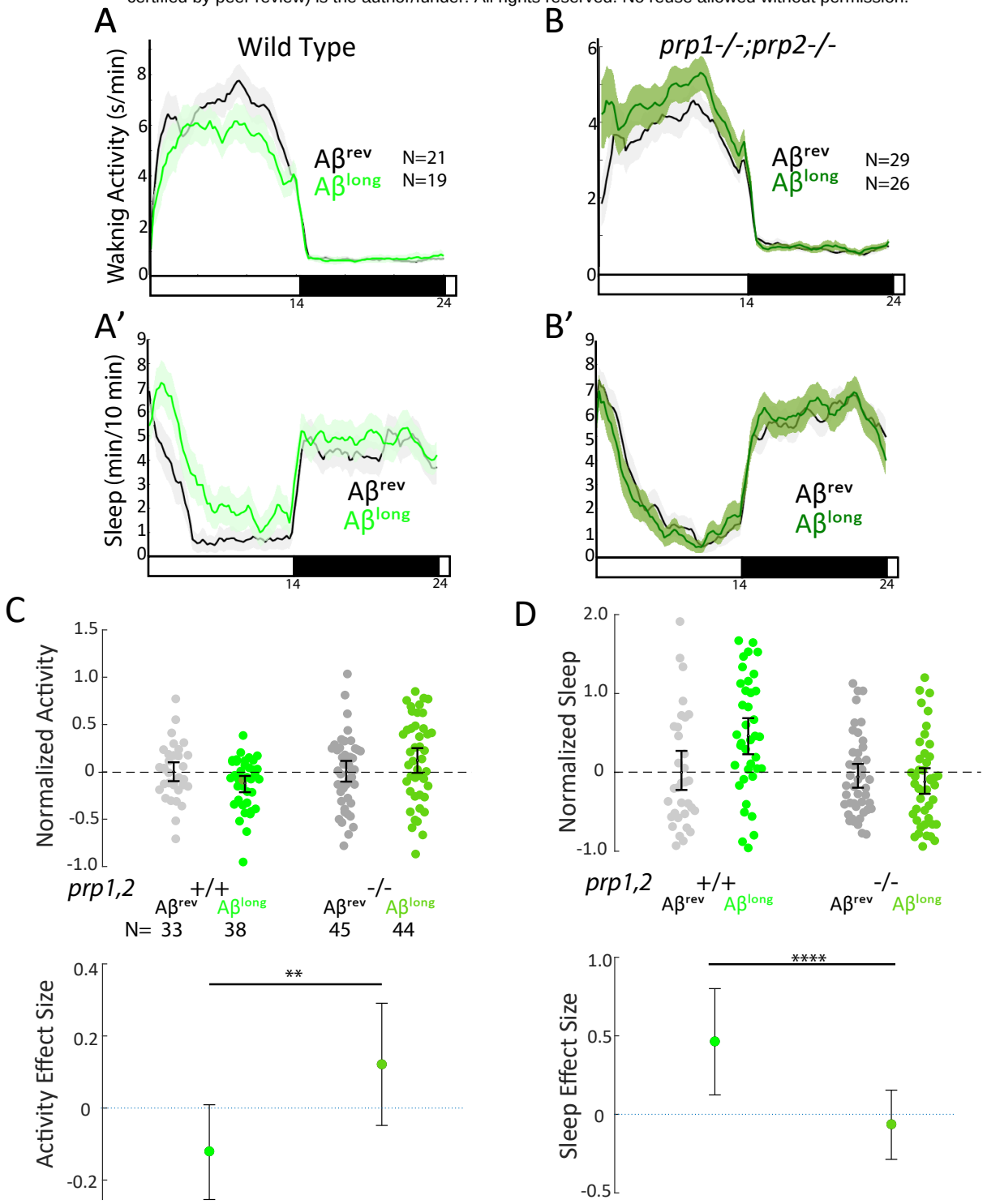

Figure 4

Figure 5

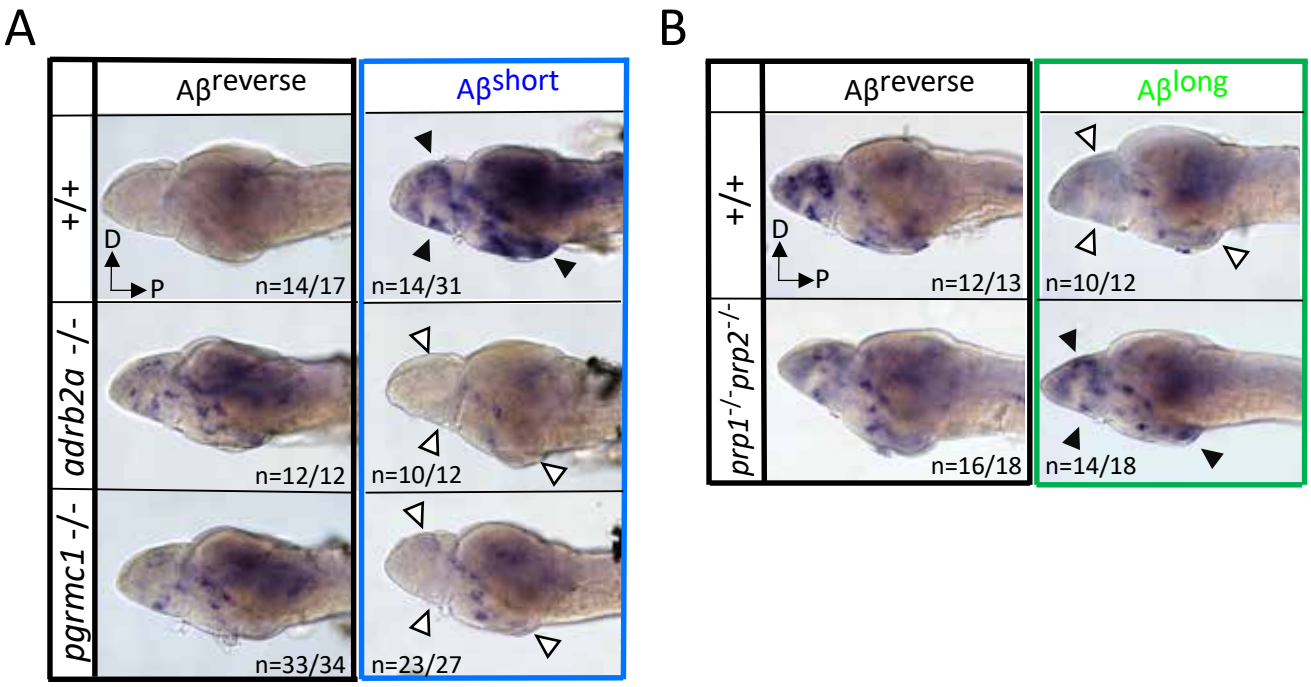

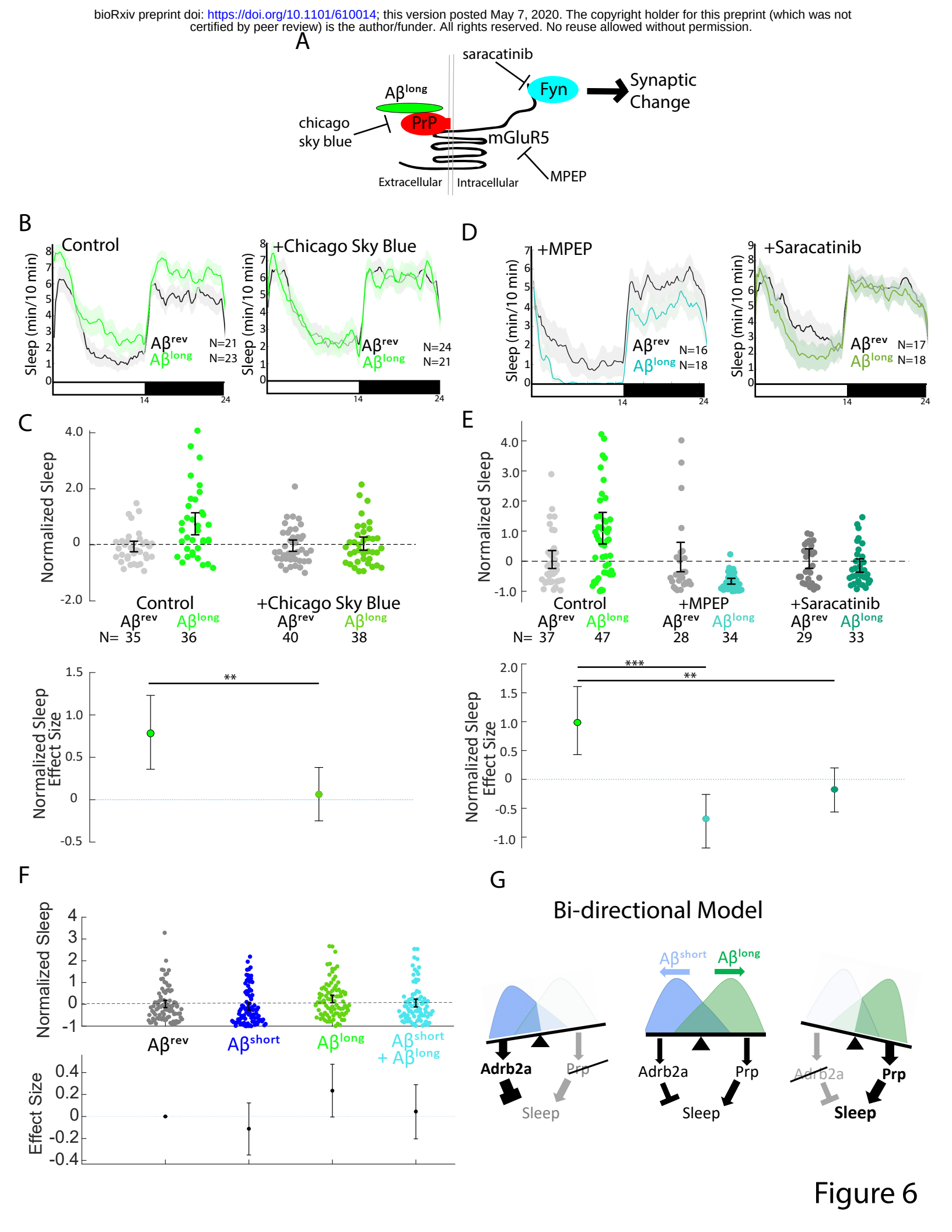

Figure 6

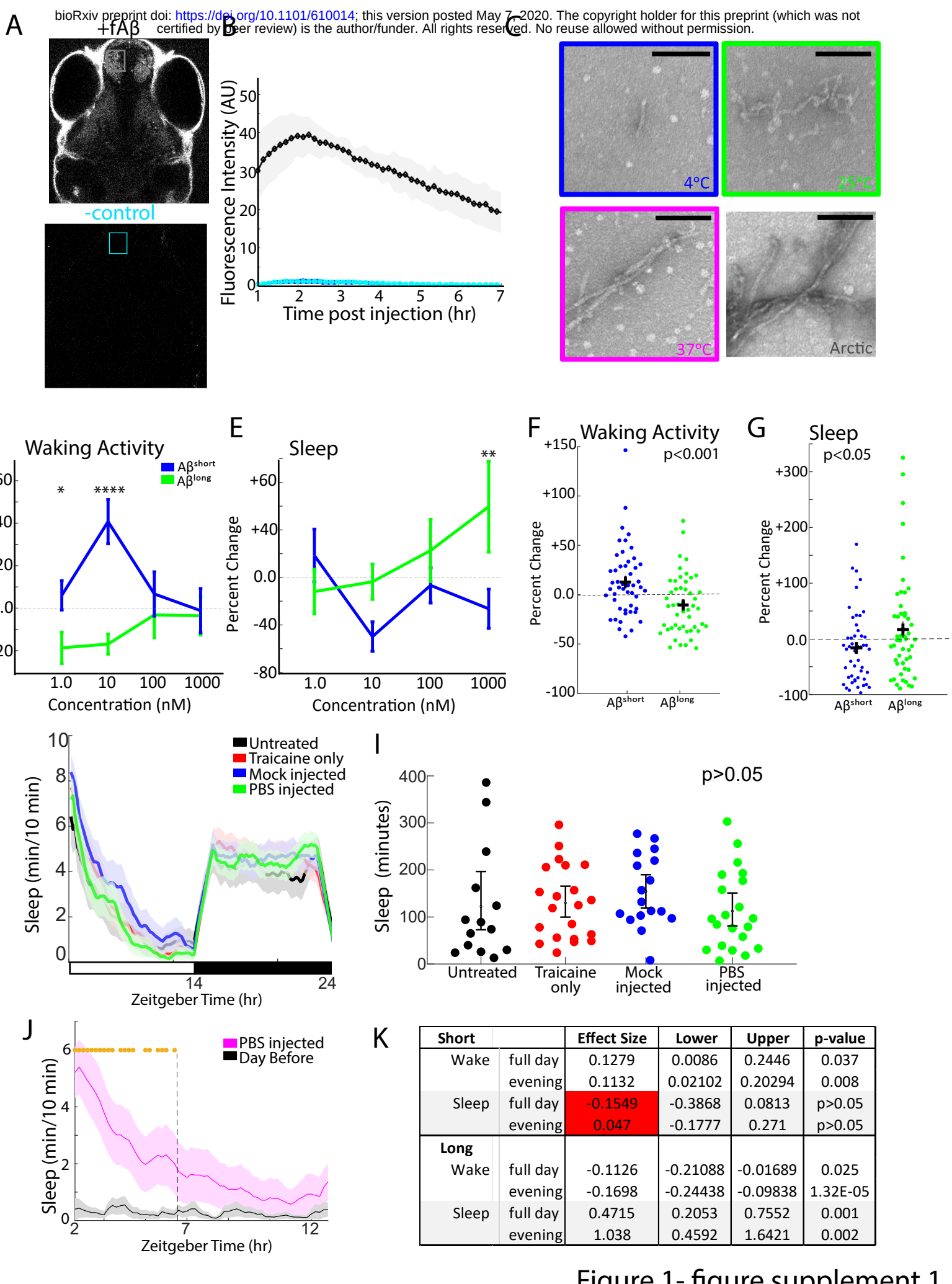

Short		Effect Size	Lower	Upper	p-value
Wake	full day	0.1279	0.0086	0.2446	0.037
	evening	0.1132	0.02102	0.20294	0.008
Sleep	full day	-0.1549	-0.3868	0.0813	p>0.05
	evening	0.047	-0.1777	0.271	p>0.05
Long					
Wake	full day	-0.1126	-0.21088	-0.01689	0.025
	evening	-0.1698	-0.24438	-0.09838	1.32E-05
Sleep	full day	0.4715	0.2053	0.7552	0.001
	evening	1.038	0.4592	1.6421	0.002

Figure 1- figure supplement 1

A.

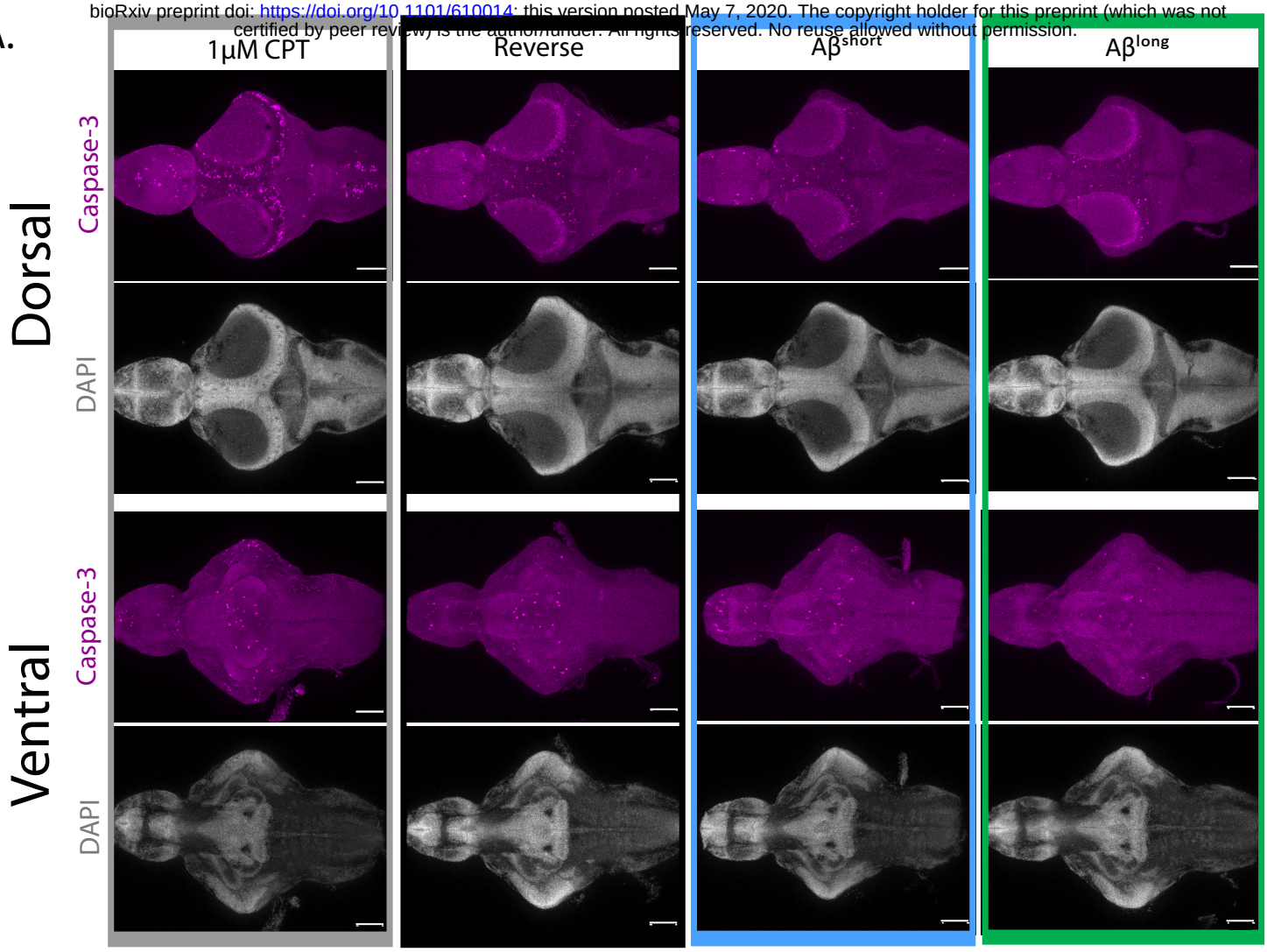

B.

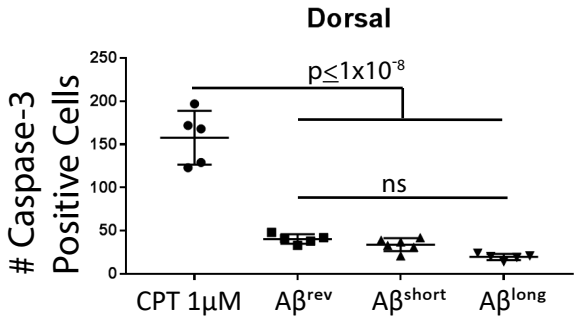

C.

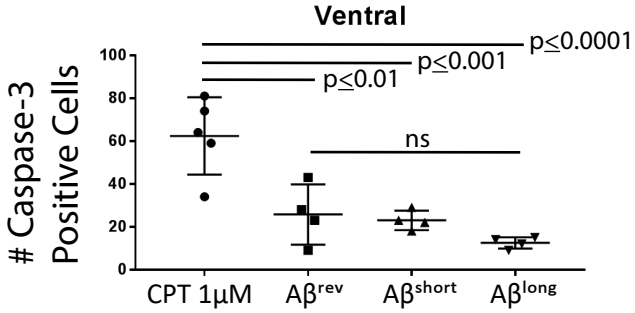

D.

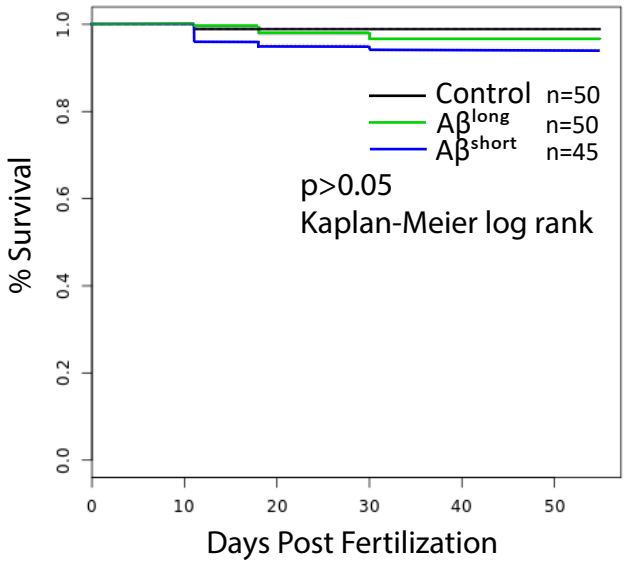

Figure 1- figure supplement 2

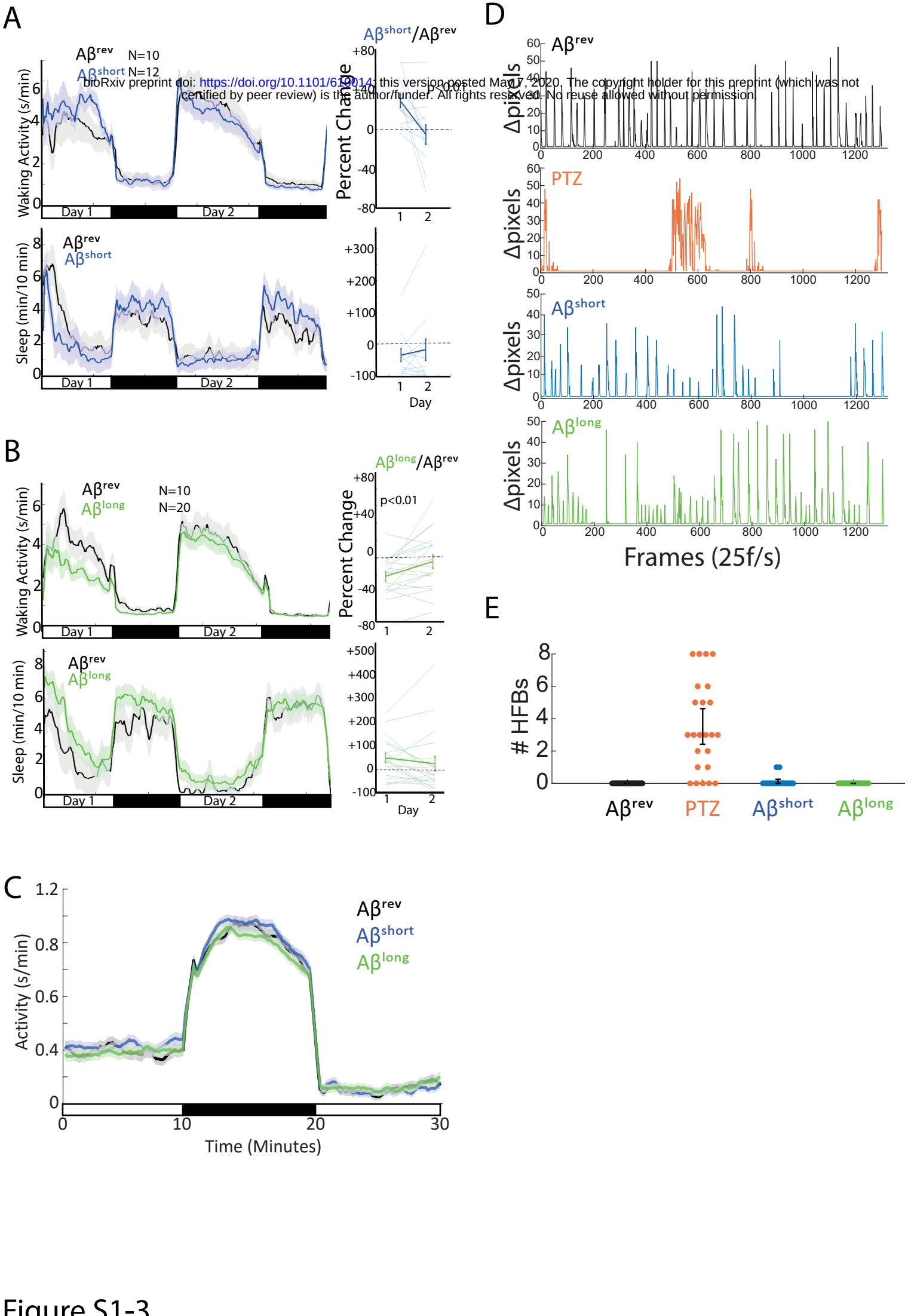

Figure S1-3

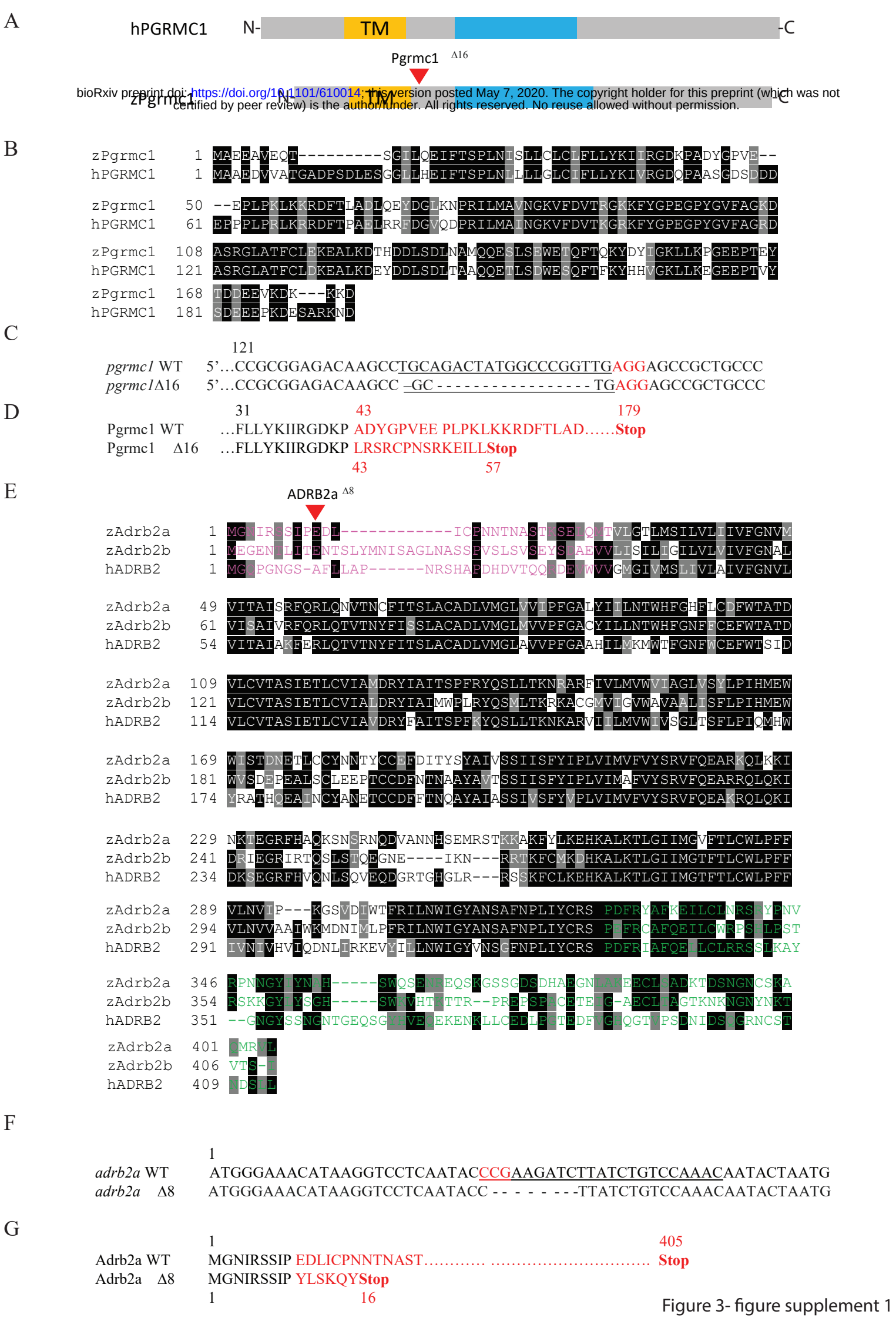

Figure 3- figure supplement 1

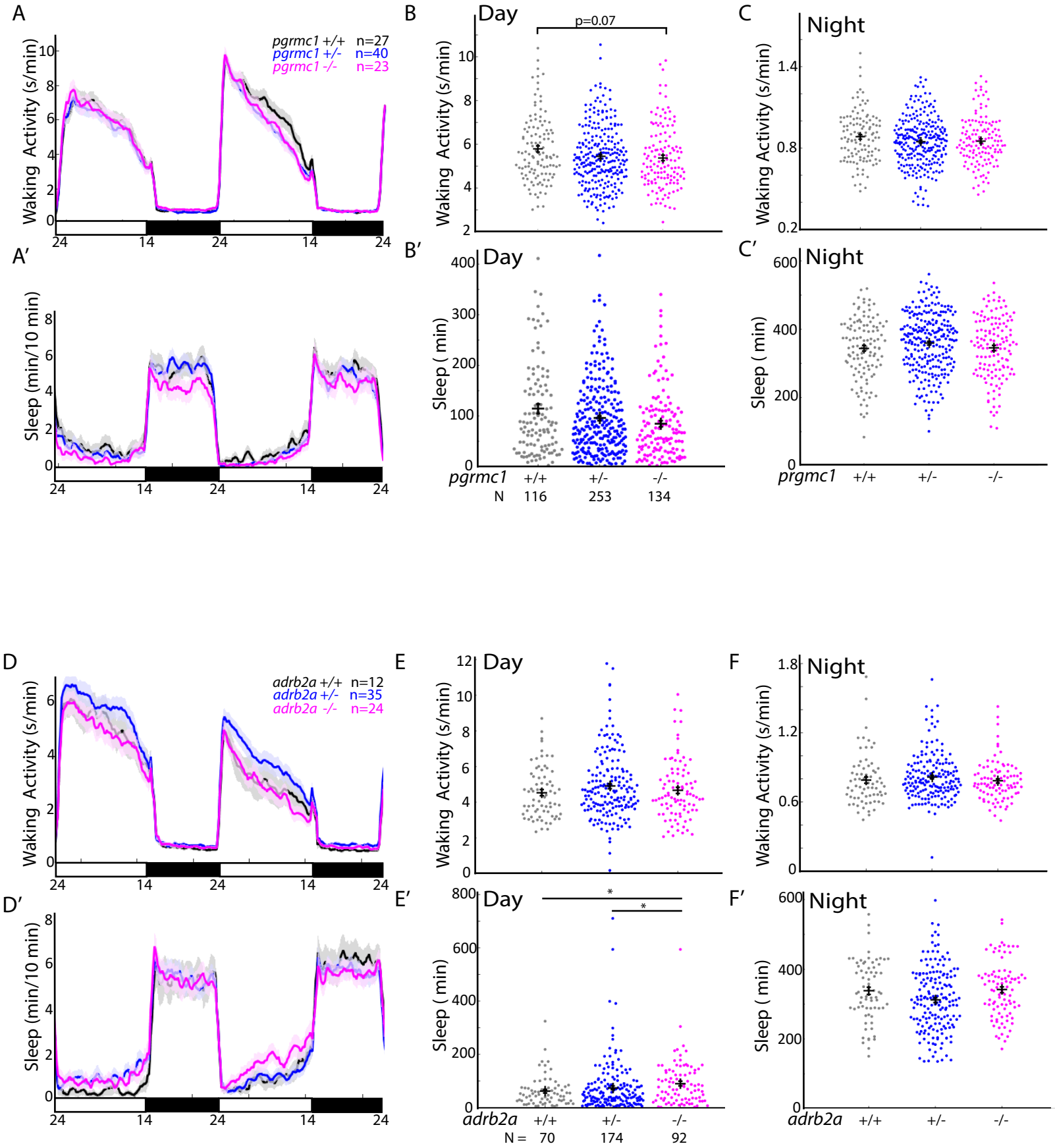

Figure 3- figure supplement 2

A

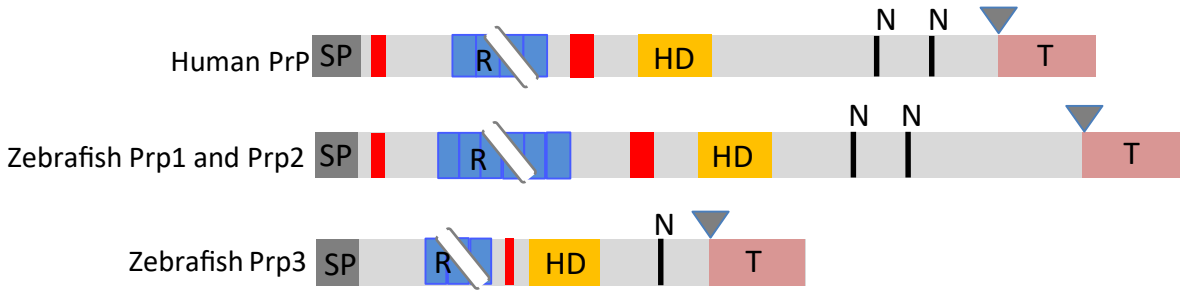

B

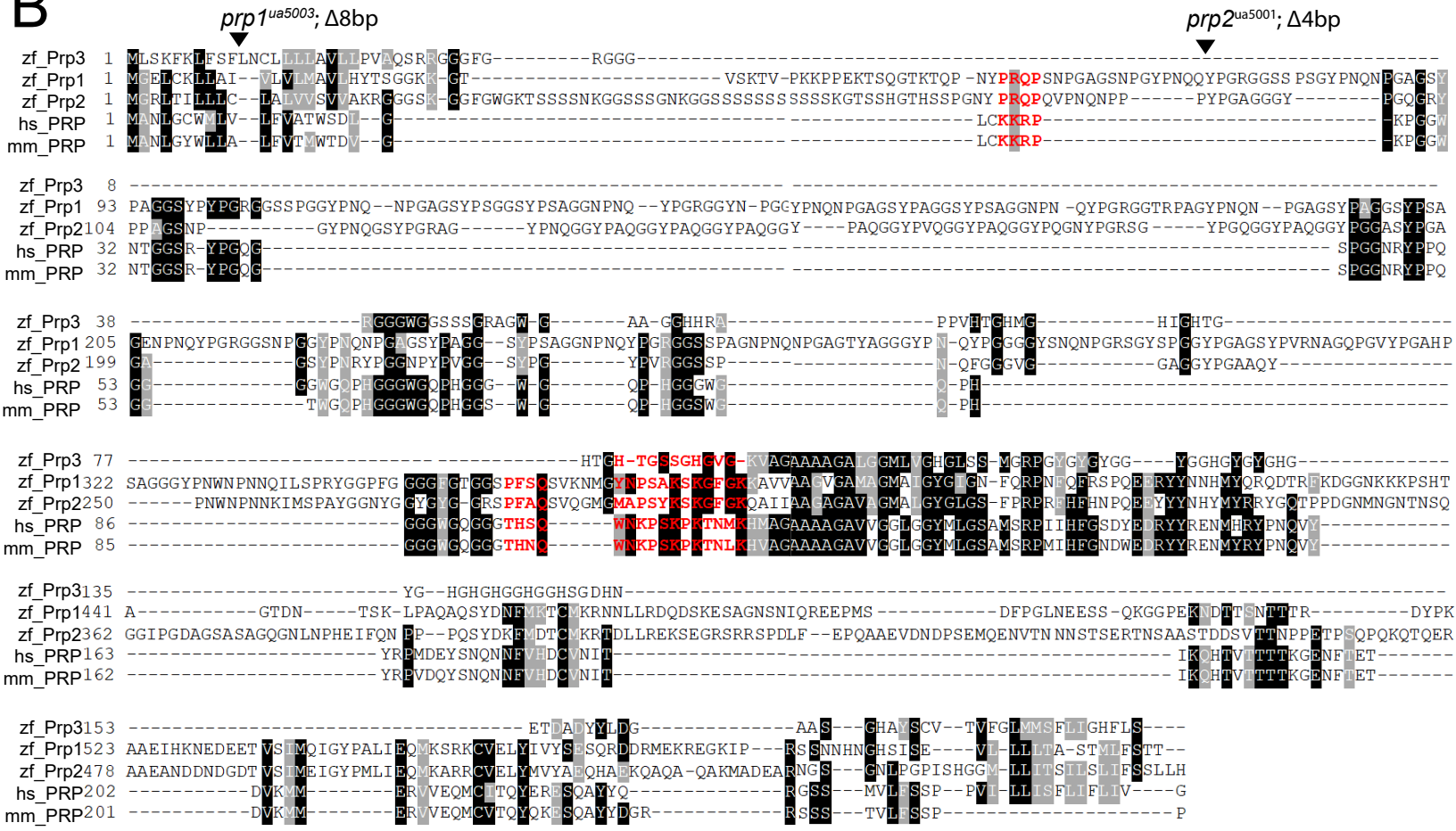

Figure 4- figure supplement 1

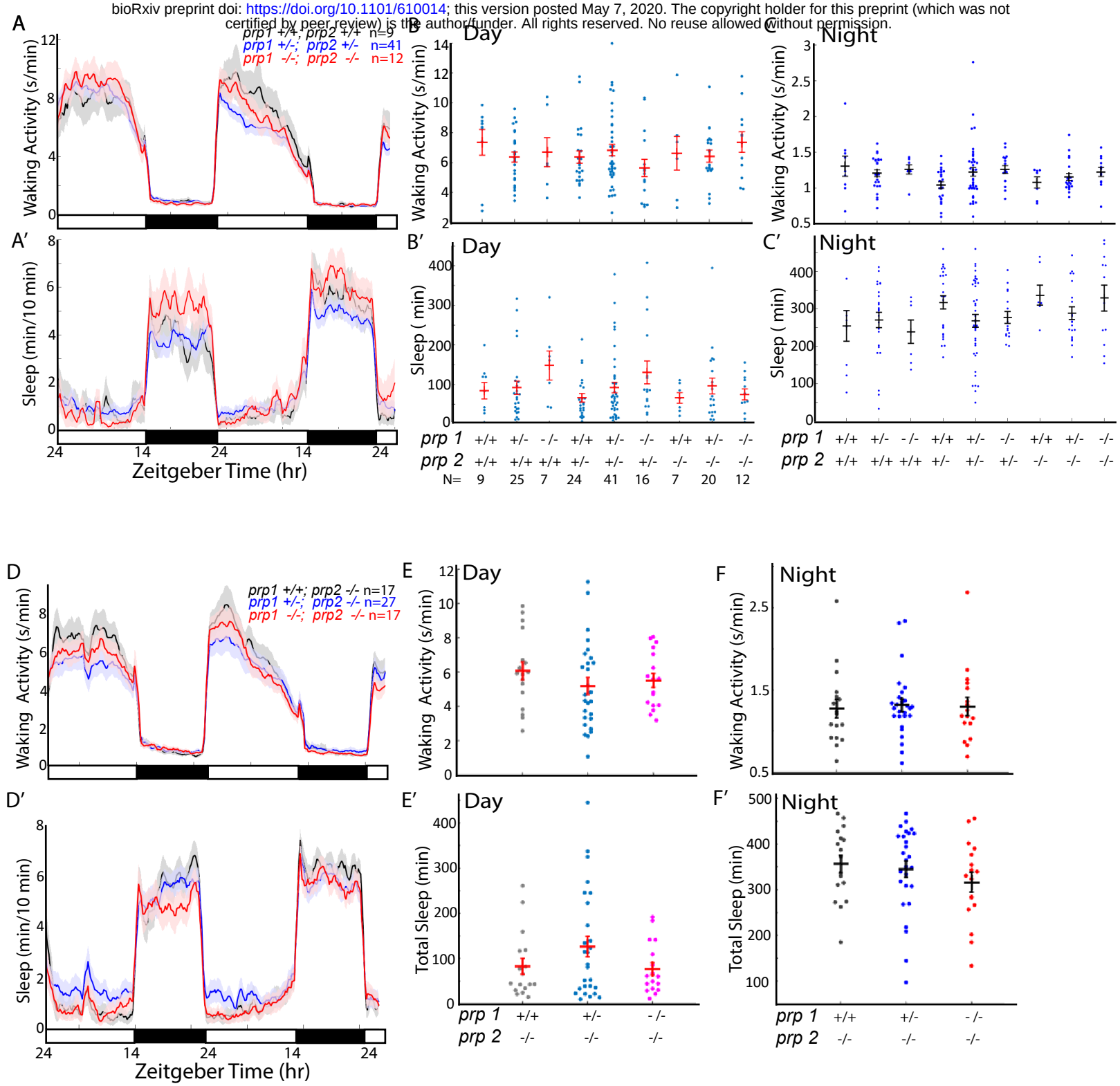

Figure 4- figure supplement 2

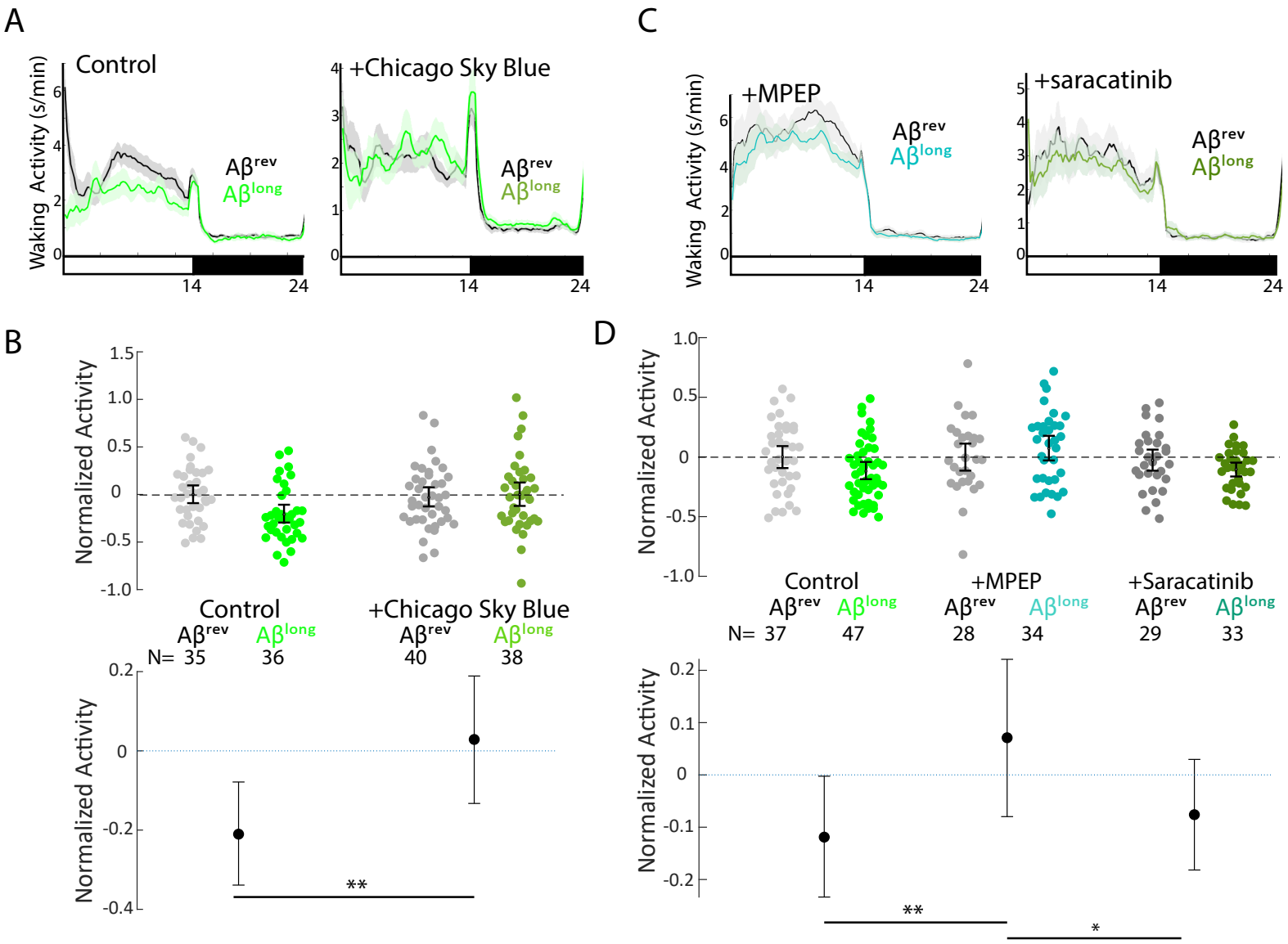

Figure 6-figure supplement 1